Full Dimensional (15D) Quantum-Dynamical Simulation of the Protonated Water-Dimer I: Hamiltonian Setup and Analysis of the Ground Vibrational State.

Oriol Vendrell, Fabien Gatti, D. Lauvergnat, H.-D. Meyer

Full Dimensional (15D) Quantum-Dynamical Simulation of the Protonated Water-Dimer I: Hamiltonian Setup and Analysis of the Ground Vibrational State

Oriol Vendrell,[1,*] Fabien Gatti,[2,†] David Lauvergnat,[3,‡] and Hans-Dieter Meyer[1,§]

[1] *Theoretische Chemie, Physikalisch-Chemisches Institut, Universität Heidelberg, INF 229, D-69120 Heidelberg, Germany*

[2] *CTMM, Institut Gerhardt (UMR 5232-CNRS), CC 1501, Université de Montpellier II, F-34095 Montpellier, Cedex 05, France*

[3] *CNRS, Laboratoire de Chimie Physique (UMR 8000), Université Paris-Sud, F-91405 Orsay*

(Dated: October 27, 2018)

Abstract

Quantum-dynamical full-dimensional (15D) calculations are reported for the protonated water dimer ($H_5O_2^+$) using the multiconfiguration time-dependent Hartree (MCTDH) method. The dynamics is described by curvilinear coordinates. The expression of the kinetic energy operator in this set of coordinates is given and its derivation, following the polyspherical method, is discussed. The PES employed is that of Huang *et al.* [JCP, **122**, 044308, (2005)]. A scheme for the representation of the potential energy surface (PES) is discussed which is based on a high dimensional model representation scheme (cut-HDMR), but modified to take advantage of the mode-combination representation of the vibrational wavefunction used in MCTDH. The convergence of the PES expansion used is quantified and evidence is provided that it correctly reproduces the reference PES at least for the range of energies of interest. The reported zero point energy of the system is converged with respect to the MCTDH expansion and in excellent agreement (16.7 cm^{-1} below) with the diffusion Monte Carlo result on the PES of Huang *et al.* The highly fluxional nature of the cation is accounted for through use of curvilinear coordinates. The system is found to interconvert between equivalent minima through wagging and internal rotation motions already when in the ground vibrational-state, i.e., T=0. It is shown that a converged quantum-dynamical description of such a flexible, multi-minima system is possible.

*e-mail: oriol.vendrell@pci.uni-heidelberg.de

†e-mail: gatti@univ-montp2.fr

‡e-mail: david.lauvergnat@lcp.u-psud.fr

§e-mail: Hans-Dieter.Meyer@pci.uni-heidelberg.de

I. INTRODUCTION

The protonated water-dimer $H_5O_2^+$ (Zundel cation) is the smallest system in which an excess proton is shared between two water molecules. Much effort has been devoted to this system due to the importance that the solvated proton has in several areas of chemistry and biology. In recent years a fast development of the spectroscopical techniques available to probe the vibrational dynamics of ionic species in the gas phase has taken place, and several studies have appeared around the $H_5O_2^+$ system [1, 2, 3, 4] and other more complex clusters and molecules [5, 6]. In order to achieve a satisfactory understanding of the spectroscopy and dynamics accurate theoretical results are needed in parallel and several works have appeared to fill this gap which are based on different theoretical approaches, from classical- to quantum-dynamical methods [4, 7, 8, 9, 10, 11]. Accurate quantum-dynamical simulations of the dynamics and spectroscopy of the system require of an accurate reference potential energy surface (PES). Very accurate PES and dipole moment surfaces (DMS) have been recently produced by Huang et al. [7] for $H_5O_2^+$. They are based on several ten-thousands of coupled-cluster calculations combined with a clever fitting algorithm which is based on a redundant set of coordinates, namely all atom-atom distances. The PES is able to describe the floppy motions occurring at typical energies of excitation in the linear IR regime and dissociates correctly [7]. Several works have already appeared in which the PES and DMS of Huang et al. [7] were used [4, 11, 12]. In Ref. [12] full-dimensional vibrational calculations for $H_5O_2^+$ were undertaken using diffusion Monte Carlo (DMC) and variational wavefunction methods. The zero point energy (ZPE), some vibrational excited-state energies and properties of the ground vibrational state of the system are reported and discussed. The PES of Huang et al. was also used in Ref. [4] where the experimental IR spectrum of the system was reported together with the calculation of relevant excited-vibrational states.

As will be later discussed, $H_5O_2^+$ features several symmetry-equivalent minimum energy structures and large amplitude motions between different regions connected by low energy barriers. For such systems curvilinear coordinates, e.g. bond-bond angle, dihedral angle, or internal rotation coordinates, offer an advantage over rectilinear coordinates since they provide a physically meaningful description of the different large-amplitude molecular motions. As a remark, an attempt was made to describe the system by a set of rectilinear coordinates, since they result in a simple expression of the kinetic energy operator (KEO). The resulting

Hamiltonian was unsuccessful at describing of variuos large-amplitude displacements, which resulted in abandonement of such an approach and introduction of a curvilinear-coordinates based Hamiltonian. When deriving the KEO for a Hamitonian in curvilinear coordinates one may define those in terms of rectilinear atom motions and use standard differential calculus to obtain the desired expression [13]. This approach becomes extremely complex and error prone already for systems of a few atoms. Another possibility is to use an approximate KEO where some cross-terms are neglected, thus simplifying the derivation. In this case, however, an uncontrolled source of error is introduced in the calculation. These drawbacks are overcome by employing the polyspherical approach [14, 15, 16] when defining the coordinate set and deriving the corresponding KEO. In the polyspherical method the system is described by a set of vectors of any kind (e.g. Jacobi, valence, ...). The kinetic energy is given in terms of the variation in length and orientation of these vectors, the latter is defined by angles with respect to a body fixed frame. Following the polyspherical method the KEO of the system at hand is derived in a systematic way without use of differential calculus. The polyspherical approach has already been discussed in a general framework as well as for some molecular systems (see for instance [14, 15, 16, 17]). In this paper the full derivation of the KEO in a set of polyspherical coordinates is illustrated for the $H_5O_2^+$ cation and all the key steps are carefully discussed. The derivation is followed step-by-step for this rather complex system, thus providing the basic guidelines to be followed for the derivation of KEOs for complex molecular systems and clusters.

In quantum-dynamical wavefunction-based studies, as the one being introduced here, it is convenient to represent the operators on a discrete variable representation (DVR) grid, which in the multidimensional case is the direct product of one-dimensional DVRs. The potential operator is then given by the value of the PES at each point of the grid. In the present case, however, the resulting primitive grid has more than 10^{15} points. This number makes clear that the potential must be represented in a more compact form to make the calculations feasible. Algorithms exist which take advantage of the fact that correlation usually involves the concerted evolution of only a small number of coordinates as compared to the total number. Hierarchical representations of the PES are then constructed including potential-function terms up to a given number of coordinates [18, 19, 20]. We discuss here a variation of a hierarchical representation of the PES in which the coordinates are grouped together into modes, and the modes are the basic units that define the hierarchical expansion.

It will be shown that this approach allows for a fast convergence of the PES representation if the modes are defined as groups of the most strongly correlated coordinates.

The present work provides new reference results on the properties of the ground vibrational state of $H_5O_2^+$. The convergence of the given results is established by comparison to the DMC results [12] on the reference PES of Huang et al. [7]. These results, together with the Hamiltonian defined here, set also the theoretical and methodological framework used in the companion paper [21] where the IR spectrum and vibrational dynamics of $H_5O_2^+$ are analyzed.

The paper is organized as follows. Section II presents a brief description of the multiconfiguration time-dependent Hartree (MCTDH) method. Section III details the construction of the Hamiltonian operator for the $H_5O_2^+$ system. The derivation of the KEO is discussed in III A, while the construction of the potential is detailed in III B. Section IV A discusses the calculation of the ground vibrational state of the system and gives a comparison to available results. In section IV B some properties of the system in relation to its ground vibrational-state wavefunction are discussed. In section IV C the quality of the potential expansion is analyzed and discussed. Section V provides some general conclusions.

II. BRIEF DESCRIPTION OF THE MCTDH METHOD

The *Multiconfiguration time-dependent Hartree* (MCTDH) method [22, 23, 24, 25] is a general algorithm to solve the time-dependent Schrödinger equation. The MCTDH wave function is expanded in a sum of products of so–called *single–particle functions* (SPFs). The SPFs, $\varphi(Q,t)$, may be one– or multi–dimensional functions and, in the latter case, the coordinate Q is a collective one, $Q = (q_k, \cdots, q_l)$. As the SPFs are time–dependent, they follow the wave packet and often a rather small number of SPFs suffices for convergence.

The *ansatz* for the MCTDH wavefunction reads

$$\begin{aligned} \Psi(q_1,\cdots,q_f,t) &\equiv \Psi(Q_1,\cdots,Q_p,t) \\ &= \sum_{j_1}^{n_1}\cdots\sum_{j_p}^{n_p} A_{j_1,\cdots,j_p}(t)\prod_{\kappa=1}^{p}\varphi_{j_\kappa}^{(\kappa)}(Q_\kappa,t) \\ &= \sum_J A_J\,\Phi_J\ , \end{aligned} \tag{1}$$

where f denotes the number of degrees of freedom and p the number of MCTDH *particles*,

also called *combined modes*. There are n_κ SPFs for the κ'th particle. The $A_J \equiv A_{j_1 \dots j_f}$ denote the MCTDH expansion coefficients and the configurations, or Hartree-products, Φ_J are products of SPFs, implicitly defined by Eq. (1). The SPFs are finally represented by linear combinations of time-independent primitive basis functions or DVR grids.

The MCTDH equations of motion are derived by applying the Dirac-Frenkel variational principle to the *ansatz* Eq. (1). After some algebra, one obtains

$$i\dot{A}_J = \sum_L \langle \Phi_J \,|\, H \,|\, \Phi_L \rangle \, A_L \,, \tag{2}$$

$$i\dot{\boldsymbol{\varphi}}^{(\kappa)} = \left(1 - P^{(\kappa)}\right) \left(\boldsymbol{\rho}^{(\kappa)}\right)^{-1} \langle \mathbf{H} \rangle^{(\kappa)} \boldsymbol{\varphi}^{(\kappa)} \,, \tag{3}$$

where a vector notation, $\boldsymbol{\varphi}^{(\kappa)} = (\varphi_1^{(\kappa)}, \cdots, \varphi_{n_\kappa}^{(\kappa)})^T$, is used. Details on the derivation, the definitions of the mean-field $\langle \mathbf{H} \rangle^{(\kappa)}$, the density $\boldsymbol{\rho}^{(\kappa)}$ and the projector $P^{(\kappa)}$, as well as more general results, can be found in Refs. [23, 24, 25]. Here and in the following (except for Section III) we use a unit system with $\hbar = 1$.

The MCTDH equations conserve the norm and, for time-independent Hamiltonians, the total energy. MCTDH simplifies to Time-Dependent Hartree when setting all $n_\kappa = 1$. Increasing the n_κ recovers more and more correlation, until finally, when n_κ equals the number of primitive functions, the standard method (i. e. propagating the wave packet on the primitive basis) is used. It is important to note, that MCTDH uses variationally optimal SPFs, because this ensures early convergence.

The solution of the equations of motion requires to build the mean–fields at every time–step. A fast evaluation of the mean–fields is hence essential. To this end the Hamiltonian is written as a sum of products of mono–particle operators:

$$H = \sum_{r=1}^{s} c_r \prod_{\kappa=1}^{p} h_r^{(\kappa)} \,, \tag{4}$$

where $h_r^{(\kappa)}$ operates on the κ-th particle only and where the c_r are numbers. In this case the matrix-elements of the Hamiltonian can be expressed by a sum of products of mono–mode integrals, the evaluation of which is fast.

$$\langle \Phi_J | H | \Phi_L \rangle = \sum_{r=1}^{s} c_r \prod_{\kappa=1}^{p} \langle \varphi_{j_\kappa} | h_r^{(\kappa)} | \varphi_{l_\kappa} \rangle \,, \tag{5}$$

Similar expressions apply to the matrix of mean-fields $\langle \mathbf{H} \rangle^{(\kappa)}$. For further information on the MCTDH method, see http://www.pci.uni-heidelberg.de/tc/usr/mctdh/.

III. SYSTEM HAMILTONIAN

A. Kinetic energy operator for $H_5O_2^+$

The derivation of the exact kinetic energy operator for $H_5O_2^+$ is based on a polyspherical approach which has been devised in previous articles [14, 15, 16, 17, 26, 27]. This approach can be seen as a very efficient way to obtain kinetic energy operators for the family of polyspherical coordinates. The formalism can be applied whatever the number of atoms and whatever the set of vectors: Jacobi, Radau, valence, satellite, etc. The formalism is not restricted to total J=0 and hence the operator may include overall rotation and Coriolis coupling.

The protonated water dimer system is described by six Jacobi vectors. The choice of the Jacobi vectors is not unique and several clustering schemes are possible, one natural choice for $H_5O_2^+$ is given in Figure 1.

FIGURE 1 AROUND HERE

The polyspherical approach straightforwardly provides the expression of the kinetic energy operator in terms of the angular momenta associated with the vectors describing the system. Here we use the technique of "separation into two subsystems" which is described in Ref. 15 (see Eq. (37) there). The full kinetic energy operator reads (we use the notation $\partial_x = \frac{\partial}{\partial x}$ and $\partial_x^2 = \frac{\partial^2}{\partial x^2}$ throughout the paper):

$$\begin{aligned}
\hat{T} &= (-\frac{\hbar^2}{2\mu_R}\frac{1}{R}\partial_R^2 R) + \frac{(\vec{J}^\dagger\cdot\vec{J} + (\vec{L}_A+\vec{L}_B+\vec{l})^2 - 2(\vec{L}_A+\vec{L}_B+\vec{l})\cdot\vec{J})_{E2}}{2\mu_R R^2} \\
&+ \sum_{i=1}^{2}(-\frac{\hbar^2}{2\mu_{iA}}\frac{1}{R_{iA}}\partial_{R_{iA}}^2 R_{iA}) + \frac{(\vec{L}_A^2 + \vec{L}_{1A}^\dagger\cdot\vec{L}_{1A} - 2\vec{L}_A\cdot\vec{L}_{1A})_{BFA}}{2\mu_{2A}R_{2A}^2} + \frac{(\vec{L}_{1A}^\dagger\cdot\vec{L}_{1A})_{BFA}}{2\mu_{1A}R_{1A}^2} \\
&+ \sum_{i=1}^{2}(-\frac{\hbar^2}{2\mu_{iB}}\frac{1}{R_{iB}}\partial_{R_{iB}}^2 R_{iB}) + \frac{(\vec{L}_B^2 + \vec{L}_{1B}^\dagger\cdot\vec{L}_{1B} - 2\vec{L}_B\cdot\vec{L}_{1B})_{BFB}}{2\mu_{2B}R_{2B}^2} + \frac{(\vec{L}_{1B}^\dagger\cdot\vec{L}_{1B})_{BFB}}{2\mu_{1B}R_{1B}^2} \\
&- \frac{\hbar^2}{2m}\frac{1}{r}\partial_r^2 r + \frac{(\vec{l}^2)_{E2}}{2mr^2}
\end{aligned} \tag{6}$$

with

- R, R_{1A}, R_{2A}, R_{1B}, R_{2B}, r, are the lengths of the vectors $\vec{R}$, $\vec{R}_{1A}$, $\vec{R}_{2A}$, $\vec{R}_{1B}$, $\vec{R}_{2B}$, $\vec{r}$, respectively.

- $\mu_{1\,A(B)} = \frac{m_O 2m_H}{m_O+2m_H}$, $\mu_{2\,A(B)} = \frac{m_H}{2}$, $\mu_R = \frac{m_O+2m_H}{2}$, and $m = \frac{2m_H(m_O+2m_H)}{2m_O+5m_H}$.

- $\vec{L}_{1\,A(B)}$ is the angular momentum associated with $\vec{R}_{1\,A(B)}$.

- $\vec{L}_{2\,A(B)}$ is the angular momentum associated with $\vec{R}_{2\,A(B)}$ and $\vec{L}_{A(B)}$ $(= \vec{L}_{1\,A(B)}+\vec{L}_{2\,A(B)})$ is the total angular momentum associated with monomer A (B).

- $\vec{l}$ is the angular momentum associated with the proton.

- $\vec{J}$ is the total angular momentum of the system. $\vec{J} = \vec{l} + \vec{L}_A + \vec{L}_B + \vec{L}_R$ and $\vec{L}_R$ is the angular momentum associated with $\vec{R}$.

- E2 is the frame resulting from the two first Euler rotations starting from the space fixed frame, such that the z^{E2} axis lies parallel to $\vec{R}$. In other words, the two first Euler angles α and β are identical to the two spherical angles of $\vec{R}$ in the space fixed frame.

- BFA (B) is the body fixed frame associated with monomer A (B). The two first Euler angles $\alpha_{A(B)}$ and $\beta_{A(B)}$ of monomer A (B) are defined such as $z^{BFA(B)}$ lies parallel to $\vec{R}_{2\,A(B)}$ (in other words they are identical to the two spherical angles of $\vec{R}_{2\,A(B)}$ in the E2 frame). The third Euler angle $\gamma_{A(B)}$ is defined such as $\vec{R}_{1\,A(B)}$ remains parallel to the $((xz)^{BFA(B)}, x^{BFA(B)} > 0)$ half plane. This definition of BFA(B) is similar to the one recently used to describe the water dimer (see e.g. Ref [28]). Note however that we have changed the definition of the $z^{BFA(B)}$ axis which is now parallel to the vector between the two hydrogen atoms and not to the vector joining the center of mass of H_2 to the oxygen atom as in Ref. [28]. This change was performed to avoid the singularity which appears in the KEO when $\vec{R}$ and $z^{BFA(B)}$ are parallel.

It should be emphasized that all the angular momenta appearing in the kinetic energy operator are all *computed* in the space fixed frame but *projected* onto the axes of different frames. This last point, as well as the properties of the corresponding projections, is addressed in detail in Ref. [29]. We recall here only the main point, i.e. the fact that if a vector is not involved in the definition of a frame F, the expression of the projections of

the corresponding angular momentum onto the F-axes in terms of the coordinates in this frame, is identical to the usual one in a space fixed frame. This very useful property will be utilized several times in the following for instance to obtain Eqs. (13,14,15,25,28,29).

We now slightly change the volume element for the lengths of the vectors (as usual), and assume J=0. The operator can then be recast in the following form:

$$\begin{aligned}\hat{T} &= (-\frac{\hbar^2}{2\mu_R}\partial_R^2) + \frac{(\vec{L}_A + \vec{L}_B + \vec{l})^2_{E2}}{2\mu_R R^2} - \frac{\hbar^2}{2m}\partial_r^2 + \frac{(\vec{l}^2)_{E2}}{2mr^2} \\ &+ \sum_{i=1}^{2}(-\frac{\hbar^2}{2\mu_{iA}}\partial_{R_{iA}}^2) + \frac{(\vec{L}_A^2 + \vec{L}_{1A}^\dagger \cdot \vec{L}_{1A} - 2\vec{L}_A \cdot \vec{L}_{1A})_{BFA}}{2\mu_{2A}R_{2A}^2} + \frac{(\vec{L}_{1A}^\dagger \cdot \vec{L}_{1A})_{BFA}}{2\mu_{1A}R_{1A}^2} \\ &+ \sum_{i=1}^{2}(-\frac{\hbar^2}{2\mu_{iB}}\partial_{R_{iB}}^2) + \frac{(\vec{L}_B^2 + \vec{L}_{1B}^\dagger \cdot \vec{L}_{1B} - 2\vec{L}_B \cdot \vec{L}_{1B})_{BFB}}{2\mu_{2B}R_{2B}^2} + \frac{(\vec{L}_{1B}^\dagger \cdot \vec{L}_{1B})_{BFB}}{2\mu_{1B}R_{1B}^2}\end{aligned} \tag{7}$$

which is to be used with the volume element :

$$dRdR_{1A}dR_{2A}dR_{1B}dR_{2B}drd\alpha_A \sin\beta_A d\beta_A d\gamma_A d\alpha_B \sin\beta_B d\beta_B d\gamma_B \sin\theta d\theta d\varphi_H \sin\theta_{1A} d\theta_{1A} \sin\theta_{1B} d\theta_{1B} \tag{8}$$

with

$$\begin{aligned} 0 \leq\ & R, R_{1A}, R_{2A}, R_{1B}, R_{2B}, r & <\ \infty \\ 0 \leq\ & \beta_A, \beta_B, \theta, \theta_{1A}, \theta_{1B} & \leq\ \pi \\ 0 \leq\ & \alpha_A, \gamma_A, \alpha_B, \gamma_B, \varphi_H & <\ 2\pi \end{aligned}$$

We have 16 degrees of freedom instead of 15 since we have not defined the third Euler angle yet. The angles are depicted in Figure 2:

FIGURE 2 AROUND HERE

- θ and φ_H are the spherical angles of the proton in the E2 frame: θ is the angle between z^{E2} and the vector $\vec{r}$, φ_H describes the rotation of $\vec{r}$ around z^{E2}.
- β_A and α_A are the spherical angles of $\vec{R}_{2A}$ in the E2 frame. The angle β_A describes the rocking motion of water A fragment while α_A describes the rotation of the water A fragment around the $\vec{R} \equiv \vec{z}_{E2}$ axis (the same for B).

- θ_{1A} and γ_A are the spherical angles of $\vec{R}_{1A}$ in the E2A frame, the E2A frame is the frame obtained after the two Euler rotations α_A and β_A with respect to the E2 frame. Consequently, θ_{1A} is the angle between $\vec{R}_{1A}$ and $\vec{R}_{2A}$ and γ_A describes the rotation of $\vec{R}_{1A}$ around $\vec{R}_{2A}$. Hence γ_A describes the wagging motion of the water A fragment (the same for B). The fact that we have used the separation into two subsystems for the two water monomers (see Eq. (37) in Ref. [15]) explains why the angles of $\vec{R}_{1A(B)}$ are defined with respect to $\vec{R}_{2A(B)}$ and not with respect to $\vec{R}$ as in the standard formulation of the polyspherical approach (see Eq. (65) in Ref. [14]). This allows us to have purely intramonomer angles instead of angles mixing the intramonomer and intermonomer motions.

Since $(\vec{L}^2_{A(B)})_{BFA(B)} = (\vec{L}^2_{A(B)})_{E2}$ (here we can use $\vec{L}^2_{A(B)}$ rather than $\vec{L}^\dagger_{A(B)}\vec{L}_{A(B)}$ since the projections of $\vec{L}_{A(B)}$ onto the axes of the E2 or BFA (B) frames are hermitian: see Eqs. (13,15,25,29) below), we can rewrite the operator as:

$$
\begin{aligned}
\hat{T} \; &= (-\frac{\hbar^2}{2\mu_R}\partial^2_R) + \sum_{i=1}^{2}(-\frac{\hbar^2}{2\mu_{iA}}\partial^2_{R_{iA}}) + \sum_{i=1}^{2}(-\frac{\hbar^2}{2\mu_{iB}}\partial^2_{R_{iB}}) - \frac{\hbar^2}{2m}\partial^2_r + \frac{(l^2)_{E2}}{2mr^2} \\
&+ \; (\vec{L}^2_A)_{BFA}(\frac{1}{2\mu_R R^2} + \frac{1}{2\mu_{2A}R^2_{2A}}) + (\vec{L}^2_B)_{BFB}(\frac{1}{2\mu_R R^2} + \frac{1}{2\mu_{2B}R^2_{2B}}) \\
&+ \; (\vec{L}^\dagger_{1A}\cdot\vec{L}_{1A})_{BFA}(\frac{1}{2\mu_{1A}R^2_{1A}} + \frac{1}{2\mu_{2A}R^2_{2A}}) + (\vec{L}^\dagger_{1B}\cdot\vec{L}_{1B})_{BFB}(\frac{1}{2\mu_{1B}R^2_{1B}} + \frac{1}{2\mu_{2B}R^2_{2B}}) \\
&- \; \frac{(\vec{L}_A\cdot\vec{L}_{1A})_{BFA}}{\mu_{2A}R^2_{2A}} - \frac{(\vec{L}_B\cdot\vec{L}_{1B})_{BFB}}{\mu_{2B}R^2_{2B}} \\
&+ \; \frac{(\vec{L}_A\cdot\vec{L}_B)_{E2}}{\mu_R R^2} + \frac{(\vec{l}^2)_{E2}}{2\mu_R R^2} + \frac{(\vec{L}_A+\vec{L}_B)\cdot\vec{l}_{E2}}{\mu_R R^2}
\end{aligned}
\tag{9}
$$

This operator could be straightforwardly used along with an adequate primitive basis set of spherical harmonics and Wigner rotation-matrix elements. However, in this work, we prefer to employ a direct product primitive basis such as a DVR for all the degrees of freedom (only because the latter basis set is numerically more efficient for our problem). We have then to explicitly express of the angular momenta in terms of the coordinates, i.e. we have to detail the following terms:

- (1) $(\vec{L}^2_A)_{BFA}$, $(\vec{L}^2_B)_{BFB}$, $(\vec{L}^\dagger_{1A}\cdot\vec{L}_{1A})_{BFA}$, $(\vec{L}^\dagger_{1B}\cdot\vec{L}_{1B})_{BFB}$

- (2) $(\vec{L}_A \cdot \vec{L}_{1A})_{BFA}$, $(\vec{L}_B \cdot \vec{L}_{1B})_{BFB}$
- (3) $(\vec{L}_A \cdot \vec{L}_B)_{E2}$
- (4) $\vec{l}^2_{E2}$
- (5) $(\vec{L}_A + \vec{L}_B) \cdot \vec{l}_{E2}$

but before doing so we have to further specify the coordinates:

- (i) to avoid the $1/r^2$ singularity we use the BF Cartesian coordinates x, y, and z for the proton (the definition of BF frame is given in (ii)). Hence we use, $\partial_{\varphi_H^{BF}} = x\partial_y - y\partial_x$.
- (ii) we slightly change the coordinate system (from E2 to BF) and explicitly define the third Euler angle γ of the system and then the BF frame. We define γ such that it is identical to the first Euler angle of monomer A (here, we slightly break the symmetry between the two monomers). Consequently, we have:

$$\begin{aligned} \gamma &= \alpha_A \\ \alpha &= \alpha_B - \alpha_A \\ \varphi_H^{BF} &= \varphi_H^{E2} - \alpha_A \end{aligned} \tag{10}$$

since J=0, we can then put:

$$\partial_\gamma = 0 \tag{11}$$

and find

$$\begin{aligned} \partial_{\alpha_A} &= -\partial_\alpha - \partial_{\varphi_H^{BF}} = -\partial_\alpha - (x\partial_y - y\partial_x) \\ \partial_{\alpha_B} &= \partial_\alpha \end{aligned} \tag{12}$$

Note that this transformation does not affect the other angles.

- (iii) in order to have hermitian conjugate momenta for the angles, we use $\mathrm{u}_{\beta_A} = \cos\beta_A$, $\mathrm{u}_{\beta_B} = \cos\beta_B$, $\mathrm{u}_{\theta_{1A}} = \cos\theta_{1A}$, $\mathrm{u}_{\theta_{1B}} = \cos\theta_{1B}$.
  For each angle η, we have (with $\mathrm{u}_\eta = \cos\eta$): $\partial_\eta = -\sin\eta\partial_{u_\eta} = -\sqrt{1-u_\eta^2}\partial_{u_\eta}$ and $\partial_\eta^\dagger = -\partial_{u_\eta}\sqrt{1-u_\eta^2}$.

We have now 15 degrees of freedom:

$$\begin{array}{rcccl} 0 & \leq & R, R_{1A}, R_{2A}, R_{1B}, R_{2B} & < & \infty \\ -1 & \leq & u_{\beta_A}, u_{\beta_B}, u_{\theta_{1A}}, u_{\theta_{1B}} & \leq & 1 \\ 0 & \leq & \alpha, \gamma_A, \gamma_B & < & 2\pi \\ -\infty & < & x, y, z & < & \infty \end{array}$$

Let us now detail all the terms appearing in the kinetic energy operator:

- (1) For $\vec{L}_{B\,BFB}$, the situation is simple since monomer B is not involved in the definition of the body fixed frame of the whole system. Thus, we have :

$$\begin{aligned} L_{B\,x^{BFB}} &= i\hbar\tfrac{\cos\gamma_B}{\sin\beta_B}\partial_{\alpha_B} + i\hbar\sin\gamma_B\sin\beta_B\partial_{u_{\beta B}} - i\hbar\tfrac{u_{\beta B}}{\sin\beta_B}\cos\gamma_B\partial_{\gamma_B} \\ L_{B\,y^{BFB}} &= -i\hbar\tfrac{\sin\gamma_B}{\sin\beta_B}\partial_{\alpha_B} + i\hbar\cos\gamma_B\sin\beta_B\partial_{u_{\beta B}} + i\hbar\tfrac{u_{\beta B}}{\sin\beta_B}\sin\gamma_B\partial_{\gamma_B} \\ L_{B\,z^{BFB}} &= -i\hbar\partial_{\gamma_B} \end{aligned} \tag{13}$$

  and

$$\vec{L}^2_{B\,BFB} = -\hbar^2(\partial_{u_{\beta_B}}(1-u^2_{\beta_B})\partial_{u_{\beta_B}} + \frac{1}{1-u^2_{\beta_B}}(\partial^2_{\alpha_B} + \partial^2_{\gamma_B} - 2u_{\beta_B}\partial_{\alpha_B}\partial_{\gamma_B})) \tag{14}$$

  Similarly $\vec{L}^2_{A\,BFA}$ can be seen as the total angular momentum of monomer A projected onto the axes of the Body fixed frame of the monomer. We obtain the usual expression:

$$\begin{aligned} L_{A\,x^{BFA}} &= i\hbar\tfrac{\cos\gamma_A}{\sin\beta_A}\partial_{\alpha_A} + i\hbar\sin\gamma_A\sin\beta_A\partial_{u_{\beta A}} - i\hbar\tfrac{u_{\beta A}}{\sin\beta_A}\cos\gamma_A\partial_{\gamma_A} \\ L_{A\,y^{BFA}} &= -i\hbar\tfrac{\sin\gamma_A}{\sin\beta_A}\partial_{\alpha_A} + i\hbar\cos\gamma_A\sin\beta_A\partial_{u_{\beta A}} + i\hbar\tfrac{u_{\beta A}}{\sin\beta_A}\sin\gamma_A\partial_{\gamma_A} \\ L_{A\,z^{BFA}} &= -i\hbar\partial_{\gamma_A} \end{aligned} \tag{15}$$

  and

$$\vec{L}^2_{A\,BFA} = -\hbar^2(\partial_{u_{\beta_A}}(1-u^2_{\beta_A})\partial_{u_{\beta_A}} + \frac{1}{1-u^2_{\beta_A}}(\partial^2_{\alpha_A} + \partial^2_{\gamma_A} - 2u_{\beta_A}\partial_{\alpha_A}\partial_{\gamma_A})) \tag{16}$$

However, since monomer A is involved in the definition of the third Euler angle of the system, we apply the change of coordinates, Eqs. (10) and (12):

$$\begin{aligned}(\partial^2_{\alpha_A} &+ \partial^2_{\gamma_A} - 2u_{\beta_A}\partial_{\alpha_A}\partial_{\gamma_A}) = \\ (\partial^2_{\alpha} &+ x^2\partial^2_y + y^2\partial^2_x - x\partial_x\partial_y y - y\partial_y\partial_x x \\ &+ 2x\partial_y\partial_\alpha - 2y\partial_x\partial_\alpha + \partial^2_{\gamma_A} + 2u_{\beta_A}\partial_\alpha\partial_{\gamma_A} \\ &+ 2u_{\beta_A}\partial_{\gamma_A}x\partial_y - 2u_{\beta_A}\partial_{\gamma_A}y\partial_x)\end{aligned} \tag{17}$$

For the projections of $\vec{R}_{1A(B)}$ onto to the BFA (B) axes, the situation is not straightforward since $\vec{R}_{1A(B)}$ is involved in the definition of BFA (B). However, since we have used the same convention for the BF frames as in our previous articles, the expressions of these projections is already known (identical to Eq. (47a) in Ref. [14] for instance):

$$\begin{aligned}L_{1A\,x^{BFA}} &= i\hbar\tfrac{u_{\theta 1A}}{\sin\theta_{1A}}\partial_{\gamma_A} \\ L_{1A\,y^{BFA}} &= i\hbar\sin\theta_{1A}\partial_{u_{\theta 1A}} \\ L_{1A\,z^{BFA}} &= -i\hbar\partial_{\gamma_A}\end{aligned} \tag{18}$$

(This expression can be obtained starting from the E2A frame which is the frame resulting from the two first Euler rotations γ_A and β_A. The expression of the projections of $\vec{L}_{1A}$ onto this E2A frame are the usual ones since $\vec{R}_{1\,A}$ is not involved in the definition of this frame. Applying then the third Euler rotation and the coordinate transformation leading to the BFA coordinates yields Eq. (18)). Note that $L_{1A\,y^{BFA}}$ is not hermitian (this is due to the fact that $\vec{R}_{1A}$ is involved in the definition of BFA). However, at the end we obtain the usual expression:

$$(\vec{L}^{\dagger}_{1A}\cdot\vec{L}_{1A})_{BFA} = -\hbar^2(\partial_{u_{\theta 1A}}(1-u^2_{\theta_{1A}})\partial_{u_{\theta 1A}} + \frac{1}{1-u^2_{\theta_{1A}}}\partial^2_{\gamma_A}) \tag{19}$$

and exactly the same for B:

$$(\vec{L}^{\dagger}_{1B}\cdot\vec{L}_{1B})_{BFB} = -\hbar^2(\partial_{u_{\theta 1B}}(1-u^2_{\theta_{1B}})\partial_{u_{\theta 1B}} + \frac{1}{1-u^2_{\theta_{1B}}}\partial^2_{\gamma_B}) \tag{20}$$

- (2) The terms in $(\vec{L}_{A(B)} \cdot \vec{L}_{1A(B)})_{BFA(B)}$ are not obvious since $\vec{R}_{1\,A(B)}$ is involved in the definition of BFA (B). First, let us explicitly highlight the hermiticity of the term:

$$(\vec{L}_A \cdot \vec{L}_{1A})_{BFA} \;=\; 1/2(\vec{L}^{\dagger}_A \cdot \vec{L}_{1A} + \vec{L}^{\dagger}_{1A} \cdot \vec{L}_A)_{BFA} \tag{21}$$

Combining Eq. (18) and Eq. (15) (as well as Eq. (10) and Eq. (12)), we obtain:

$$\begin{aligned}
&(\vec{L}_A \cdot \vec{L}_{1A})_{BFA} = \\
&- \frac{\hbar^2}{2}[-(\partial_\alpha + x\partial_y - y\partial_x)\frac{u_{\theta_{1A}}}{\sin\theta_{1A}}\frac{\cos\gamma_A}{\sin\beta_A}\partial_{\gamma_A} \\
&+ \partial_{u_{\beta_A}}\frac{u_{\theta_{1A}}}{\sin\theta_{1A}}\sin\beta_A\sin\gamma_A\partial_{\gamma_A} - 2\partial_{\gamma_A}\frac{u_{\beta_A}}{\sin\beta_A}\cos\gamma_A\frac{u_{\theta_{1A}}}{\sin\theta_{1A}}\partial_{\gamma_A} \\
&+ 2\partial^2_{\gamma_A} + (\partial_\alpha + x\partial_y - y\partial_x)\frac{\sin\gamma_A}{\sin\beta_A}\sin\theta_{1A}\partial_{u_{\theta_{1A}}} \\
&+ \partial_{u_{\beta_A}}\sin\beta_A\cos\gamma_A\sin\theta_{1A}\partial_{u_{\theta_{1A}}} + \partial_{\gamma_A}\frac{u_{\beta_A}}{\sin\beta_A}\sin\gamma_A\sin\theta_{1A}\partial_{u_{\theta_{1A}}} \\
&- \partial_{\gamma_A}\frac{u_{\theta_{1A}}}{\sin\theta_{1A}}\frac{\cos\gamma_A}{\sin\beta_A}(\partial_\alpha + x\partial_y - y\partial_x) + \partial_{\gamma_A}\frac{u_{\theta_{1A}}}{\sin\theta_{1A}}\sin\beta_A\sin\gamma_A\partial_{u_{\beta_A}} \qquad (22) \\
&+ \partial_{u_{\theta_{1A}}}\frac{\sin\gamma_A}{\sin\beta_A}\sin\theta_{1A}(\partial_\alpha + x\partial_y - y\partial_x) \\
&+ \partial_{u_{\theta_{1A}}}\sin\beta_A\cos\gamma_A\sin\theta_{1A}\partial_{u_{\beta_A}} + \partial_{u_{\theta_{1A}}}\frac{u_{\beta_A}}{\sin\beta_A}\sin\gamma_A\sin\theta_{1A}\partial_{\gamma_A}]
\end{aligned} \tag{23}$$

and for B (the situation is a little bit simpler since monomer B is not involved in the definition of the third Euler angle see Eq. (12)):

$$\begin{aligned}
&(\vec{L}_B \cdot \vec{L}_{1B})_{BFB} = \\
&- \frac{\hbar^2}{2}[\partial_\alpha\frac{u_{\theta_{1B}}}{\sin\theta_{1B}}\frac{\cos\gamma_B}{\sin\beta_B}\partial_{\gamma_B} + \partial_{u_{\beta_B}}\frac{u_{\theta_{1B}}}{\sin\theta_{1B}}\sin\beta_B\sin\gamma_B\partial_{\gamma_B} - 2\partial_{\gamma_B}\frac{u_{\theta_{1B}}}{\sin\theta_{1B}}\cos\gamma_B\frac{u_{\beta_B}}{\sin\beta_B}\partial_{\gamma_B} \\
&+ 2\partial^2_{\gamma_B} - \partial_\alpha\frac{\sin\gamma_B}{\sin\beta_B}\sin\theta_{1B}\partial_{u_{\theta_{1B}}} + \partial_{u_{\beta_B}}\sin\beta_B\cos\gamma_B\sin\theta_{1B}\partial_{u_{\theta_{1B}}} + \partial_{\gamma_B}\frac{u_{\beta_B}}{\sin\beta_B}\sin\gamma_B\sin\theta_{1B}\partial_{u_{\theta_{1B}}} \\
&+ \partial_{\gamma_B}\frac{u_{\theta_{1B}}}{\sin\theta_{1B}}\frac{\cos\gamma_B}{\sin\beta_B}\partial_\alpha + \partial_{\gamma_B}\frac{u_{\theta_{1B}}}{\sin\theta_{1B}}\sin\beta_B\sin\gamma_B\partial_{u_{\beta_B}} \\
&- \partial_{u_{\theta_{1B}}}\frac{\sin\gamma_B}{\sin\beta_B}\sin\theta_{1B}\partial_\alpha + \partial_{u_{\theta_{1B}}}\sin\beta_B\cos\gamma_B\sin\theta_{1B}\partial_{u_{\beta_B}} \\
&+ \partial_{u_{\theta_{1B}}}\frac{u_{\beta_B}}{\sin\beta_B}\sin\gamma_B\sin\theta_{1B}\partial_{\gamma_B}]
\end{aligned} \tag{24}$$

- (3) For the term in $1/2(\vec{L}_A^{\dagger} \cdot \vec{L}_B)_{E2}$, we note that the expression of the projections of $\vec{L}_{A(B)}$ onto the E2 can be seen as those of total angular momentum of a system onto the axes of the Space fixed frame. Indeed, since monomers A and B are not involved in the definition of E2, we have (similar to Eq. (18) in Ref. [14]):

$$\begin{aligned} L_{A\,x^{E2}} &= i\hbar \cos\alpha_A \tfrac{u_A}{\sin\beta_A}\partial_{\alpha_A} - i\hbar \sin\alpha_A \sin\beta_A \partial_{u_{\beta A}} - i\hbar \tfrac{\cos\alpha_A}{\sin\beta_A}\partial_{\gamma_A} \\ L_{A\,y^{E2}} &= i\hbar \sin\alpha_A \tfrac{u_A}{\sin\beta_A}\partial_{\alpha_A} + i\hbar \cos\alpha_A \sin\beta_A \partial_{u_{\beta A}} - i\hbar \tfrac{\sin\alpha_A}{\sin\beta_A}\partial_{\gamma_A} \\ L_{A\,z^{E2}} &= -i\hbar\partial_{\alpha_A} \end{aligned} \tag{25}$$

After, noticing that

$$(\vec{L}_A \cdot \vec{L}_B)_{E2} \;=\; \frac{1}{2}(\vec{L}_A^{\dagger} \cdot \vec{L}_B + \vec{L}_B^{\dagger} \cdot \vec{L}_A)_{E2} \tag{26}$$

we obtain after using Eq. (12):

$$\begin{aligned} &\frac{1}{2}(\vec{L}_A^{\dagger} \cdot \vec{L}_B)_{E2} = -\frac{\hbar^2}{2}[-\partial_\alpha \cos\alpha \frac{u_{\beta_A}}{\sin\beta_A}\frac{u_{\beta_B}}{\sin\beta_B}\partial_\alpha \\ -\;& (x\partial_y - y\partial_x)\cos\alpha \frac{u_{\beta_A}}{\sin\beta_A}\frac{u_{\beta_B}}{\sin\beta_B}\partial_\alpha \\ +\;& \partial_{\gamma_A}\frac{\cos\alpha}{\sin\beta_A\sin\beta_B}\partial_{\gamma_B} + \partial_\alpha \sin\alpha \frac{u_{\beta_A}}{\sin\beta_A}\sin\beta_B\partial_{u_{\beta_B}} + (x\partial_y - y\partial_x)\sin\alpha\frac{u_{\beta_A}}{\sin\beta_A}\sin\beta_B\partial_{u_{\beta_B}} \\ +\;& \partial_\alpha \cos\alpha \frac{u_{\beta_A}}{\sin\beta_A}\frac{1}{\sin\beta_B}\partial_{\gamma_B} + \partial_{u_{\beta_A}}\sin\alpha\sin\beta_A\frac{u_{\beta_B}}{\sin\beta_B}\partial_\alpha \\ +\;& (x\partial_y - y\partial_x)\cos\alpha\frac{u_{\beta_A}}{\sin\beta_A}\frac{1}{\sin\beta_B}\partial_{\gamma_B} \\ +\;& \partial_{u_{\beta_A}}\cos\alpha\sin\beta_A\sin\beta_B\partial_{u_{\beta_B}} - \partial_{u_{\beta_A}}\sin\alpha\frac{\sin\beta_A}{\sin\beta_B}\partial_{\gamma_B} \\ -\;& \partial_{\gamma_A}\cos\alpha\frac{1}{\sin\beta_A}\frac{u_{\beta_B}}{\sin\beta_B}\partial_\alpha + \partial_{\gamma_A}\sin\alpha\frac{\sin\beta_B}{\sin\beta_A}\partial_{u_{\beta_B}} - \partial_\alpha^2 - \partial_\alpha(x\partial_y - y\partial_x)] \end{aligned} \tag{27}$$

- (4) Since the proton is not involved in the definition of the whole body fixed frame, the expression of the projections of $\hat{\vec{l}}$ onto the E_2 (or BF) axes is the usual one. At the end, we obtain:

$$\begin{aligned} (\vec{l})^2_{E2} \;=\; (\vec{l})^2_{BF} = -\hbar^2(&y^2\partial_z^2 + z^2\partial_y^2 + z^2\partial_x^2 + x^2\partial_z^2 + x^2\partial_y^2 + y^2\partial_x^2 \\ &-y\partial_y\partial_z z - \partial_y y z\partial_z - \partial_x x z\partial_z - x\partial_x\partial_z z - x\partial_x\partial_y y - \partial_x x y\partial_y) \end{aligned} \tag{28}$$

- (5) For the last term $(\vec{L}_A + \vec{L}_B) \cdot \vec{l}_{E2} = (\vec{L}_A + \vec{L}_B)^\dagger \cdot \vec{l} + \vec{l}^\dagger \cdot (\vec{L}_A + \vec{L}_B)_{BF}$, we need to know the expression of the projections of $\vec{L}_{A(B)}$ onto the body fixed axes. For $\vec{L}_B$, there is no particular problem since B is not involved in the definition of γ and thus of the BF frame:

$$\begin{aligned} L_{B\,x^{BF}} &= i\hbar \tfrac{u_{\beta B}}{\sin\beta_B} \cos\alpha \partial_\alpha - i\hbar \sin\alpha \sin\beta_B \partial_{u_{\beta B}} - i\hbar \tfrac{\cos\alpha}{\sin\beta_B \beta_B} \partial_{\gamma_B} \\ L_{B\,y^{BF}} &= i\hbar \sin\alpha \tfrac{u_{\beta B}}{\sin\beta_B} \partial_\alpha + i\hbar \cos\alpha \sin\beta_B \partial_{u_{\beta B}} - i\hbar \tfrac{\sin\alpha}{\sin\beta_B} \partial_{\gamma_B} \\ L_{B\,z^{BF}} &= -i\hbar \partial_\alpha \end{aligned} \tag{29}$$

  For $\vec{L}_A$, it is less straightforward. However, applying the third Euler rotation to Eq. (25) and using Eq. (12) yields:

$$\begin{aligned} L_{A\,x^{BF}} &= -i \tfrac{u_{\beta A}}{\sin\beta_A} (\partial_\alpha + x\partial_y - y\partial_x) - \tfrac{i}{\sin\beta_A} \partial_{\gamma_A} \\ L_{A\,y^{BF}} &= i \sin\beta_A \partial_{u_{\beta A}} \\ L_{A\,z^{BF}} &= i(\partial_\alpha + x\partial_y - y\partial_x) \end{aligned} \tag{30}$$

  and thus:

$$\begin{aligned} (\vec{L}_A + \vec{L}_B) \cdot \vec{l}_{E2} \;=\; & \frac{1}{2}((\vec{L}_A + \vec{L}_B)^\dagger \cdot \vec{l} + \vec{l}^\dagger \cdot (\vec{L}_A + \vec{L}_B))_{BF} = \frac{\hbar^2}{2}[(-2\frac{u_{\beta A}}{\sin\beta_A}\partial_\alpha - 2\frac{1}{\sin\beta_A}\partial_{\gamma_A} \\ &+ \frac{u_{\beta B}}{\sin\beta_B}\cos\alpha\partial_\alpha + \partial\alpha\frac{u_{\beta B}}{\sin\beta_B}\cos\alpha - \sin\alpha\sin\beta_B\partial_{u_{\beta B}} \\ &- \partial_{u_{\beta B}}\sin\alpha\sin\beta_B - 2\frac{\cos\alpha}{\sin\beta_B}\partial_{\gamma_B})(y\partial_z - z\partial_y) \\ &+ (\sin\beta_A\partial_{u_A} + \partial_{u_{\beta A}}\sin\beta_A \\ &+ \sin\alpha\frac{u_{\beta B}}{\sin\beta_B}\partial_\alpha + \partial_\alpha\sin\alpha\frac{u_B}{\sin\beta_B} + \cos\alpha\sin\beta_B\partial_{u_{\beta B}} \\ &+ \partial_{u_{\beta B}}\cos\alpha\sin\beta_B - 2\frac{\sin\alpha}{\sin\beta_B}\partial_{\gamma_B})(z\partial_x - x\partial_z) \\ &+ 2(x^2\partial_y^2 + y^2\partial_x^2 - x\partial_x\partial_y y - \partial_x x y\partial_y)] \\ &- \hbar^2[\frac{u_A}{\sin\beta_A}(x\partial_y y\partial_z + xy\partial_y\partial_z - 2x\partial_y^2 z - 2\partial_x y^2\partial_z + \partial_x y\partial_y z + \partial_x\partial_y yz)] \end{aligned} \tag{31}$$

The final expression of the operator in Eq. (9) is recast as $\hat{T} = \hat{T}_1 + \hat{T}_2 + \hat{T}_3 + \hat{T}_4$ with

$$
\begin{aligned}
\hat{T}_1 &= (-\frac{\hbar^2}{2\mu_R}\frac{\partial^2}{\partial_R^2}) + \sum_{i=1}^{2}(-\frac{\hbar^2}{2\mu_{iA}}\frac{\partial^2}{\partial_{R_{iA}}^2}) + \sum_{i=1}^{2}(-\frac{\hbar^2}{2\mu_{iB}}\frac{\partial^2}{\partial_{R_{iB}}^2}) - \frac{\hbar^2}{2m}\frac{\partial^2}{\partial_r^2} + \frac{(l^2)_{E2}}{2mr^2} \\
&+ (\vec{L}_A^2)_{BFA}(\frac{1}{2\mu_R R^2} + \frac{1}{2\mu_{2A}R_{2A}^2}) + (\vec{L}_B^2)_{BFB}(\frac{1}{2\mu_R R^2} + \frac{1}{2\mu_{2B}R_{2B}^2}) \\
&+ (\vec{L}_{1A}^{\dagger} \cdot \vec{L}_{1A})_{BFA}(\frac{1}{2\mu_{1A}R_{1A}^2} + \frac{1}{2\mu_{2A}R_{2A}^2}) + (\vec{L}_{1B}^{\dagger} \cdot \vec{L}_{1B})_{BFB}(\frac{1}{2\mu_{1B}R_{1B}^2} + \frac{1}{2\mu_{2B}R_{2B}^2})
\end{aligned}
\tag{32}
$$

$$
\hat{T}_2 = -\frac{(\vec{L}_A \cdot \vec{L}_{1A})_{BFA}}{\mu_{2A}R_{2A}^2} - \frac{(\vec{L}_B \cdot \vec{L}_{1B})_{BFB}}{\mu_{2B}R_{2B}^2}
\tag{33}
$$

$$
\hat{T}_3 = \frac{(\vec{L}_A \cdot \vec{L}_B)_{E2}}{\mu_R R^2}
\tag{34}
$$

$$
\hat{T}_4 = \frac{(\vec{l}^2)_{E2}}{2\mu_R} + \frac{(\vec{L}_A + \vec{L}_B) \cdot \vec{l}_{E2}}{\mu_R R^2}
\tag{35}
$$

The expression of the operator in terms of the 15 degrees of freedom: $R, R_{1A}, R_{2A}, R_{1B}, R_{2B}, x, y, z, \alpha, u_{\beta_A}, \gamma_A, u_{\beta_B}, \gamma_B, u_{\theta_{1A}}, u_{\theta_{1B}}$ reads: (note that the hermiticity clearly appears)

$$
\begin{aligned}
\hat{T}_1 &= (-\frac{\hbar^2}{2\mu_R}\partial_R^2) + \sum_{i=1}^{2}(-\frac{\hbar^2}{2\mu_{iA}}\partial_{R_{iA}}^2) + \sum_{i=1}^{2}(-\frac{\hbar^2}{2\mu_{iB}}\partial_{R_{iB}}^2) - \frac{\hbar^2}{2m}(\partial_x^2 + \partial_y^2 + \partial_z^2) \\
&- \hbar^2(\partial_{u_{\beta_A}}(1-u_{\beta_A}^2)\partial_{u_{\beta_A}} + \frac{1}{1-u_{\beta_A}^2}(\partial_\alpha^2 + x^2\partial_y^2 + y^2\partial_x^2 - x\partial_x\partial_y y - y\partial_y\partial_x x \\
&+ 2x\partial_y\partial_\alpha - 2y\partial_x\partial_\alpha + \partial_{\gamma_A}^2 + 2u_{\beta_A}\partial_\alpha\partial_{\gamma_A} \\
&+ 2u_{\beta_A}\partial_{\gamma_A}x\partial_y - 2u_{\beta_A}\partial_{\gamma_A}y\partial_x))(\frac{1}{2\mu_R R^2} + \frac{1}{2\mu_{2A}R_{2A}^2}) \\
&- \hbar^2(\partial_{u_{\beta_B}}(1-u_{\beta_B}^2)\partial_{u_{\beta_B}} + \frac{1}{1-u_{\beta_B}^2}(\partial_\alpha^2 + \partial_{\gamma_B}^2 - 2u_{\beta_B}\partial_\alpha\partial_{\gamma_B}))(\frac{1}{2\mu_R R^2} + \frac{1}{2\mu_{2B}R_{2B}^2}) \\
&- \hbar^2(\partial_{u_{\theta 1A}}(1-u_{\theta_{1A}}^2)\partial_{u_{\theta 1A}} + \frac{1}{1-u_{\theta_{1A}}}\partial_{\gamma_A}^2)(\frac{1}{2\mu_{1A}R_{1A}^2} + \frac{1}{2\mu_{2A}R_{2A}^2}) \\
&- \hbar^2(\partial_{u_{\theta 1B}}(1-u_{\theta_{1B}}^2)\partial_{u_{\theta 1B}} + \frac{1}{1-u_{\theta_{1B}}}\partial_{\gamma_B}^2)(\frac{1}{2\mu_{1B}R_{1B}^2} + \frac{1}{2\mu_{2B}R_{2B}^2})
\end{aligned}
\tag{36}
$$

$$
\begin{aligned}
\hat{T}_2 = \quad & \frac{\hbar^2}{2\mu_{2A}R_{2A}^2}[-(\partial_\alpha + (x\partial_y - y\partial_x))\frac{u_{\theta_{1A}}}{\sin\theta_{1A}}\frac{\cos\gamma_A}{\sin\beta_A}\partial_{\gamma_A} \\
+ \; & \partial_{u_{\beta_A}}\frac{u_{\theta_{1A}}}{\sin\theta_{1A}}\sin\beta_A\sin\gamma_A\partial_{\gamma_A} - 2\partial_{\gamma_A}\frac{u_{\beta_A}}{\sin\beta_A}\cos\gamma_A\frac{u_{\theta_{1A}}}{\sin\theta_{1A}}\partial_{\gamma_A} \\
+ \; & 2\partial_{\gamma_A}^2 + (\partial_\alpha + (x\partial_y - y\partial_x))\frac{\sin\gamma_A}{\sin\beta_A}\sin\theta_{1A}\partial_{u_{\theta_{1A}}} \\
+ \; & \partial_{u_{\beta_A}}\sin\beta_A\cos\gamma_A\sin\theta_{1A}\partial_{u_{\theta_{1A}}} + \partial_{\gamma_A}\frac{u_{\beta_A}}{\sin\beta_A}\sin\gamma_A\sin\theta_{1A}\partial_{u_{\theta_{1A}}} \\
- \; & \partial_{\gamma_A}\frac{u_{\theta_{1A}}}{\sin\theta_{1A}}\frac{\cos\gamma_A}{\sin\beta_A}(\partial_\alpha + (x\partial_y - y\partial_x)) \\
+ \; & \partial_{\gamma_A}\frac{u_{\theta_{1A}}}{\sin\theta_{1A}}\sin\beta_A\sin\gamma_A\partial_{u_{\beta_A}} \qquad (37) \\
+ \; & \partial_{u_{\theta_{1A}}}\frac{\sin\gamma_A}{\sin\beta_A}\sin\theta_{1a}(\partial_\alpha + (x\partial_y - y\partial_x)) \\
+ \; & \partial_{u_{\theta_{1a}}}\sin\beta_A\cos\gamma_A\sin\theta_{1A}\partial_{u_{\beta_A}} + \partial_{u_{\theta_{1A}}}\frac{u_{\beta_A}}{\sin\beta_A}\sin\gamma_A\sin\theta_{1A}\partial_{\gamma_A}] \\
+ \; & \frac{\hbar^2}{2\mu_{2B}R_{2B}^2}[\partial_\alpha\frac{u_{\theta_{1B}}}{\sin\theta_{1B}}\frac{\cos\gamma_B}{\sin\beta_B}\partial_{\gamma_B} + \partial_{u_{\beta_B}}\frac{u_{\theta_{1B}}}{\sin\theta_{1B}}\sin\beta_B\sin\gamma_B\partial_{\gamma_B} \\
- \; & 2\partial_{\gamma_B}\frac{u_{\theta_{1B}}}{\sin\theta_{1B}}\cos\gamma_B\frac{u_{\beta_B}}{\sin\beta_B}\partial_{\gamma_B} \\
+ \; & 2\partial_{\gamma_B}^2 - \partial_\alpha\frac{\sin\gamma_B}{\sin\beta_B}\sin\theta_{1B}\partial_{u_{\theta_{1B}}} + \partial_{u_{\beta_B}}\sin\beta_B\cos\gamma_B\sin\theta_{1B}\partial_{u_{\theta_{1B}}} \\
+ \; & \partial_{\gamma_B}\frac{u_{\beta_B}}{\sin\beta_B}\sin\gamma_B\sin\theta_{1B}\partial_{u_{\theta_{1B}}} \\
+ \; & \partial_{\gamma_B}\frac{u_{\theta_{1B}}}{\sin\theta_{1B}}\frac{\cos\gamma_B}{\sin\beta_B}\partial_\alpha + \partial_{\gamma_B}\frac{u_{\theta_{1B}}}{\sin\theta_{1B}}\sin\beta_B\sin\gamma_B\partial_{u_{\beta_B}} \\
- \; & \partial_{u_{\theta_{1B}}}\frac{\sin\gamma_B}{\sin\beta_B}\sin\theta_{1B}\partial_\alpha + \partial_{u_{\theta_{1B}}}\sin\beta_B\cos\gamma_B\sin\theta_{1B}\partial_{u_{\beta_B}} \\
+ \; & \partial_{u_{\theta_{1B}}}\frac{u_{\beta_B}}{\sin\beta_B}\sin\gamma_B\sin\theta_{1B}\partial_{\gamma_B}] \qquad (38)
\end{aligned}
$$

$$
\begin{aligned}
\hat{T}_3 \;=\; & \frac{\hbar^2}{2}[-2\partial_\alpha \cos\alpha \frac{u_{\beta_A}}{\sin\beta_A}\frac{u_{\beta_B}}{\sin\beta_B}\partial_\alpha \\
& - (x\partial_y - y\partial_x)\cos\alpha \frac{u_{\beta_A}}{\sin\beta_A}\frac{u_{\beta_B}}{\sin\beta_B}\partial_\alpha \\
& - \partial_\alpha \cos\alpha \frac{u_{\beta_A}}{\sin\beta_A}\frac{u_{\beta_B}}{\sin\beta_B}(x\partial_y - y\partial_x) \\
& + 2\partial_{\gamma_A}\frac{\cos\alpha}{\sin\beta_A\sin\beta_B}\partial_{\gamma_B} + \partial_\alpha \sin\alpha \frac{u_{\beta_A}}{\sin\beta_A}\sin\beta_B\partial_{u_{\beta_B}} \\
& + \partial_{u_{\beta_B}}\sin\alpha\frac{u_{\beta_A}}{\sin\beta_A}\sin\beta_B\partial_\alpha + (x\partial_y - y\partial_x)\sin\alpha\frac{u_{\beta_A}}{\sin\beta_A}\sin\beta_B\partial_{u_{\beta_B}} \\
& + \partial_{u_{\beta_B}}\sin\alpha\frac{u_{\beta_A}}{\sin\beta_A}\sin\beta_B(x\partial_y - y\partial_x) \\
& + \partial_\alpha\cos\alpha\frac{u_{\beta_A}}{\sin\beta_A}\frac{1}{\sin\beta_B}\partial_{\gamma_B} + \partial_{\gamma_B}\cos\alpha\frac{u_{\beta_A}}{\sin\beta_A}\frac{1}{\sin\beta_B}\partial_\alpha \\
& + \partial_{u_{\beta_A}}\sin\alpha\sin\beta_A\frac{u_{\beta_B}}{\sin\beta_B}\partial_\alpha + \partial_\alpha\sin\alpha\sin\beta_A\frac{u_{\beta_B}}{\sin\beta_B}\partial_{u_{\beta_A}} \\
& + 2(x\partial_y - y\partial_x)\cos\alpha\frac{u_{\beta_A}}{\sin\beta_A}\frac{1}{\sin\beta_B}\partial_{\gamma_B} \\
& + \partial_{u_{\beta_A}}\cos\alpha\sin\beta_A\sin\beta_B\partial_{u_{\beta_B}} + \partial_{u_{\beta_B}}\cos\alpha\sin\beta_A\sin\beta_B\partial_{u_{\beta_A}} \\
& - \partial_{u_{\beta_A}}\sin\alpha\frac{\sin\beta_A}{\sin\beta_B}\partial_{\gamma_B} - \partial_{\gamma_B}\sin\alpha\frac{\sin\beta_A}{\sin\beta_B}\partial_{u_{\beta_A}} \\
& - \partial_{\gamma_A}\cos\alpha\frac{1}{\sin\beta_A}\frac{u_{\beta_B}}{\sin\beta_B}\partial_\alpha - \partial_\alpha\cos\alpha\frac{1}{\sin\beta_A}\frac{u_{\beta_B}}{\sin\beta_B}\partial_{\gamma_A} \\
& + \partial_{\gamma_A}\sin\alpha\frac{\sin\beta_B}{\sin\beta_A}\partial_{u_{\beta_B}} + \partial_{u_{\beta_B}}\sin\alpha\frac{\sin\beta_B}{\sin\beta_A}\partial_{\gamma_A} \\
& - 2\partial_\alpha^2 - 2\partial_\alpha(x\partial_y - y\partial_x)]
\end{aligned}
\tag{39}
$$

$$
\begin{aligned}
\hat{T}_4 \;=\; & \frac{1}{2\mu_R R^2}(y^2\partial_z^2 + z^2\partial_y^2 + z^2\partial_x^2 + x^2\partial_z^2 + x^2\partial_y^2 + y^2\partial_x^2 \\
& -y\partial_y\partial_z z - \partial_y yz\partial_z - \partial_x xz\partial_z - x\partial_x\partial_z z - x\partial_x\partial_y y - \partial_x xy\partial_y) \\
+\; & \frac{1}{2\mu_R R^2}[(-2\frac{u_{\beta A}}{\sin\beta_A}\partial_\alpha - 2\frac{1}{\sin\beta_A}\partial_{\gamma_A} \\
+\; & \frac{u_{\beta B}}{\sin\beta_B}\cos\alpha\partial_\alpha + \partial_\alpha\frac{u_{\beta B}}{\sin\beta_B}\cos\alpha - \sin\alpha\sin\beta_B\partial_{u_{\beta B}} - \partial_{u_{\beta B}}\sin\alpha\sin\beta_B - 2\frac{\cos\alpha}{\sin\beta_B}\partial_{\gamma_B}) \\
& (y\partial_z - z\partial_y) \\
+\; & (\sin\beta_A\partial_{u_{\beta A}} + \partial_{u_{\beta A}}\sin\beta_A \\
+\; & \sin\alpha\frac{u_{\beta B}}{\sin\beta_B}\partial_\alpha + \partial_\alpha\sin\alpha\frac{u_{\beta B}}{\sin\beta_B} + \cos\alpha\sin\beta_B\partial_{u_{\beta B}} + \partial_{u_{\beta B}}\cos\alpha\sin\beta_B - 2\frac{\sin\alpha}{\sin\beta_B}\partial_{\gamma_B}) \\
& (z\partial_x - x\partial_z) \\
+\; & 2(x^2\partial_y^2 + y^2\partial_x^2 - x\partial_x\partial_y y - \partial_x xy\partial_y)] \\
-\; & \frac{1}{2\mu_R R^2}[\frac{u_{\beta A}}{\sin\beta_A}(x\partial_y y\partial_z + xy\partial_y\partial_z - 2x\partial_y^2 z - 2\partial_x y^2\partial_z + \partial_x y\partial_y z + \partial_x\partial_y yz)]
\end{aligned}
\tag{40}
$$

This completes the derivation of the kinetic energy operator of $H_5O_2^+$. We emphasize again that this operator is exact. Furthermore, the correctness of the derivation and implementation of the KEO was checked by comparing it with numerical results provided by the program TNUM [30]. A KEO can formally be written as $\hat{T} = (1/2)\sum_{ij} G_{ij}(\mathbf{q})\partial_i\partial_j + \sum_j F_j(\mathbf{q})\partial_j + V_{extra}(\mathbf{q})$. TNUM computes G, F and V_{extra} numerically. We have checked that the numerical values of all the functions $G_{ij}(\mathbf{q})$ at several non-symmetrical grid points $\mathbf{q}$ agree with those provided by the program TNUM. The functions $F_j(\mathbf{q})$ are determined through the hermiticity of the KEO. As our KEO is obviusly hermitian, there is no need to check the F_j.

B. Hierarchical Representation of the Potential using Mode-Combination

The exact PES ($v(\mathbf{q})$) for $H_5O_2^+$ is a function of the 15 internal coordinates previously defined, where "exact" refers to the full dimensional PES of Bowman and collaborators [7]. The calculation of vibrational levels or the IR spectrum requires a high accuracy in the representation of the Hamiltonian. The exact and trivial representation of $v(\mathbf{q})$ on a product grid is unfortunately beyond current computational capabilities: in this case the potential would be given on a grid of $\approx 10^{15}$ points ($\approx 10^4$ TB of disk space). A direct use of the

potential is hence impossible and in particular it is impossible to convert the potential to MCTDH product form by using the potfit algorithm [31, 32] since the full product grid is needed for such a transformation. The problem of representing a high-dimensional PES for quantum-dynamical computation has already been considered in the context of Multimode simulations [18], as well as in the more general context of the high dimensional model representation (HDMR) [19, 33, 34, 35].

In such hierarchical representations a multidimensional function dependent on f variables is approximated as:

$$\tilde{v}(\mathbf{q}) = v^{(0)} + \sum_{\alpha=1}^{f} v_{\alpha}^{(1)}(q_\alpha) + \sum_{\alpha<\beta}^{f} v_{\alpha\beta}^{(2)}(q_\alpha, q_\beta) + \sum_{\alpha<\beta<\gamma}^{f} v_{\alpha\beta\gamma}^{(3)}(q_\alpha, q_\beta, q_\gamma) \cdots \tag{41}$$

where $\mathbf{q}$ is a coordinate vector and $\tilde{v}(\mathbf{q})$ denotes the hierarchical approximation to $v(\mathbf{q})$. The component functions in Eq. (41) can be determined by minimizing the functional [33, 35]

$$\int_D \left[v(\mathbf{q}) - \tilde{v}(\mathbf{q})\right]^2 w(\mathbf{q}) d\mathbf{q}, \tag{42}$$

where $w(\mathbf{q})$ is some weight function on the integration domain that determines the form of the component functions. Taking $w(\mathbf{q}) = \prod_{\kappa}^{f} w_\kappa(q_\kappa)$ leads to component functions of the form [33, 34, 35, 36]

$$v^{(0)} = \int_D \prod_{\kappa=1}^{f} w_\kappa(q_\kappa) v(\mathbf{q})\, d\mathbf{q} \tag{43a}$$

$$v_{\alpha}^{(1)}(q_\alpha) = \int_{Df-1} \prod_{\kappa\neq\alpha}^{f} w_\kappa(q_\kappa) v(\mathbf{q})\, d\mathbf{q}^{\alpha} - v^{(0)} \tag{43b}$$

$$v_{\alpha\beta}^{(2)}(q_\alpha, q_\beta) = \int_{Df-2} \prod_{\kappa\neq\alpha,\beta}^{f} w_\kappa(q_\kappa) v(\mathbf{q})\, d\mathbf{q}^{\alpha\beta} - v_{\alpha}^{(1)}(q_\alpha) - v_{\alpha}^{(1)}(q_\alpha) - v^{(0)} \tag{43c}$$

$$\cdots$$

There $\mathbf{q}^{\alpha}$ represents a vector of coordinates in which the α-th component has been removed, $\mathbf{q}^{\alpha\beta}$ represents a vector in which α and β components have been removed, and so on. Non-separable weights have also been considered, which lead to more complicated expressions for component functions (see for example the Appendix in Ref. 35). It is possible to evaluate the integrals in Eq. (43) by random sampling of the coordinate space, leading to the so called RS-HDMR [33, 34, 35, 36]. However, the cumbersome multi-dimensional integrals

can be solved trivially by choosing the particular weight

$$w(\mathbf{q}) = \prod_{\alpha=1}^{f} \delta(q_\alpha - a_\alpha) \tag{44}$$

which corresponds to the cut-HDMR approximation [18, 19, 20, 33]. There a_α is the α-th component of point $\mathbf{a}$, the reference expansion point in coordinate space. Using the definition of $w(\mathbf{q})$ in Eq. (44), the different terms in Eq. (41), which we will also refer to as uncombined clusters (UC), are given up to second order by [20]

$$v^{(0)} = v(\mathbf{a}) \tag{45a}$$

$$v_\alpha^{(1)}(q_\alpha) = v(q_\alpha; \mathbf{a}^\alpha) - v^{(0)} \tag{45b}$$

$$v_{\alpha\beta}^{(2)}(q_\alpha, q_\beta) = v(q_\alpha, q_\beta; \mathbf{a}^{\alpha\beta}) - v_\alpha^{(1)}(q_\alpha) - v_\beta^{(1)}(q_\beta) - v^{(0)}, \tag{45c}$$

where higher orders follow trivially. Cut-HDMR representations of a PES – also called n-mode representation – have been already used successfully to accurately compute vibrational energy-levels of molecular systems [18, 37] and reaction rates for molecule-surface scattering [38]. Unfortunately, the use of a HDMR representation of the PES of the form of Eq. (41) leads to a combinatorial increase in the number of terms as the order of correlation increases. At the same time, higher order terms are given on grids with an exponentially increasing number of points, which leads to quick stagnation in the maximum correlation order that can be practically included.

Instead of directly adopting the expression in Eq. (41) for $v(\mathbf{q})$ we make use of the fact that the wavefunction in Eq. (1) is given in terms of combined modes. Hence we define the potential also as a function of the combined modes. The use of combined modes instead of coordinates as base of the hierarchical expansion attenuates the combinatorial increase in complexity found when using Eq. (41) while still retaining the simple evaluation of the expansion terms given by Eq. (45) and the inclusion of high-order correlations.

For f coordinates $\mathbf{q} = [q_1, \ldots, q_f]$, p particles or combined modes $\mathbf{Q} = [Q_1, \ldots, Q_p]$ are defined, such that $Q_i = [q_1^{(i)}, \ldots, q_{f_i}^{(i)}]$ and $\sum_{i=1}^{p} f_i = f$. The reference potential can be equivalently given as a function of the combined modes, $V(\mathbf{Q}) \equiv v(\mathbf{q})$. The general hierarchical expansion of Eq. (41) is now written in terms of the combined modes Q_i, instead of coordinates q_α, which up to second order reads:

$$\tilde{V}(\mathbf{Q}) = V_0 + \sum_i V_i^{(1)}(Q_i) + \sum_{ij} V_{ij}^{(2)}(Q_i, Q_j). \tag{46}$$

First order $V_i^{(1)}$ and second order $V_{ij}^{(2)}$ combined clusters (CC) are defined in an analogous way to Eq. (45):

$$V^{(0)} = V(\mathbf{a}) \tag{47a}$$

$$V_i^{(1)}(Q_i) = V(Q_i;\mathbf{a}^i) - V_0 \tag{47b}$$

$$V_{ij}^{(2)}(Q_i,Q_j) = V(Q_i,Q_j;\mathbf{a}^{ij}) - V_i^{(1)}(Q_i) - V_j^{(1)}(Q_j) - V_0 \tag{47c}$$

First order CC can be given directly in multidimensional product-grids which are direct products of the corresponding 1D DVR grids since the wavepacket is expanded in sums of products of SPFs which are defined on the same combined grids as used in the cluster expansion. Second order and higher CC are conveniently and accurately represented as sums of products of multidimensional mode-functions by employing the potfit-algorithm [31, 32].

On the other hand, first order CC can be exactly represented as a cut-HDMR expansion of the form of Eq. (41) up to order f_i in terms of the UC made of the coordinates $[q_1^{(i)}, q_2^{(i)}, \ldots]$ in Q_i, while analogously, second order CC can be given by a cut-HDMR expansion up to order $f_i + f_j$ in terms of the corresponding UC. When inspecting the expansion in Eq. (46) one realizes that the correlation between three coordinates belonging to different modes, i.e. $[q_\alpha^{(i)}, q_\beta^{(j)}, q_\gamma^{(k)}]$, is accounted for up to second order with respect to the uncombined representation since only the UC $v_{\alpha\beta}^{(2)}(q_\alpha^{(i)}, q_\beta^{(j)})$, $v_{\alpha\gamma}^{(2)}(q_\alpha^{(i)}, q_\gamma^{(k)})$ and $v_{\beta\gamma}^{(2)}(q_\beta^{(j)}, q_\gamma^{(k)})$ are contained in the second-order CC $V_{ij}^{(2)}(Q_i,Q_j)$, $V_{ik}^{(2)}(Q_i,Q_k)$ and $V_{jk}^{(2)}(Q_j,Q_k)$ respectively. Thus, using a second order expansion of CC one implicitely introduces a cluster-selection scheme of higher (up to $f_i + f_j$) order UC. The higher-order cluster-selection scheme is determined by how coordinates are grouped together into combined modes. The same reasoning can be extended to higher than second order CC. By combining coordinates which are strongly coupled it is then possible to get a high-accuracy potential while still using a reduced number of CC.

FIGURE 3 AROUND HERE

Assuming that the grid representation of each coordinate uses on average N points, the number of points in coordinate-space, N_{tot}, used to define the UC, i.e. without mode combination, is given by

$$N_{tot} = \sum_{\alpha=0}^{h} \binom{f}{\alpha} N^\alpha, \tag{48}$$

where h is the maximum allowed order for the clusters and f is the number of degrees of freedom. In case the coordinates are combined into modes with m coordinates each, the

number of grid points needed to represent the clusters is given by

$$N_{tot} = \sum_{i=0}^{h/m} \binom{f/m}{i} N^{i \cdot m}. \tag{49}$$

The number of points N for different values of the parameters defining different clustering schemes is depicted in Fig. 3. The horizontal axis represents h, the maximum order of clustering in terms of the uncombined coordinates, i.e., the maximum order of the UC in the expansion. A total of $f = 15$ coordinates is assumed. A horizontal line is drawn at 10^8, which, tentatively, constitutes a practical limit to the total number of grid points that can be used both concerning the generation of the clusters and their subsequent use in the dynamical calculations. The example in Fig. 3 assumes that there are $N = 10$ points per coordinate. Using 3D modes it is possible to include 6th order UC with around 10^7 grid points, which is of the order of the PES presented in section III C. The inclusion of up to 5th order UC without mode-combination would require more than 10^8 points while the inclusion of 6th order UC would require around 10^{10} points. We emphasize again, however, that the representations up to order h with and without mode-combination are not equivalent. The representation without mode-combination contains *all* the possible UC of coordinates up to order h. In the case of using CC one is implicitly selecting a subset of UC. A definition of meaningful mode combinations should however be possible in most cases. Such a definition would be based on chemical common-sense, e.g., coordinates belonging to the same chemical group or to the same molecule in a cluster are good candidates to be combined. As a final remark, we note that there is ongoing effort by other groups [34, 35] to use parametrized functions instead of grids to describe the clusters. This approach may turn out to be more efficient than a grid representation.

C. Potential Energy Surface for the $H_5O_2^+$ cation

In order to construct the PES for the $H_5O_2^+$ cation employing the approach described above one must start by defining the combined modes that are going to be used. In the present case the following five multidimensional modes are selected: $Q_1 = [z, \alpha, x, y]$, $Q_2 = [\gamma_A, \gamma_B]$, $Q_3 = [R, u_{\beta_A}, u_{\beta_B}]$, $Q_4 = [R_{1A}, R_{2A}, u_{\theta_{1A}}]$ and $Q_5 = [R_{1B}, R_{2B}, u_{\theta_{1B}}]$. It is convenient that coordinates x, y and α are grouped together due to symmetry conserving reasons which are exposed below. Modes Q_2 and Q_3 contain the wagging and rocking coordinates,

respectively. Modes Q_4 and Q_5 contain the Jacobi coordinates which represent the internal configuration of each water molecule. Coordinates z and R are good candidates to be combined together, as will be discussed in Section IV C. They are not combined here since this would require the definition of a 6th mode. We have, in fact, started to do some tests with a 6 particle mode-combination, and we give some brief remark on this below. The definition of the underlying 1D grids is provided in Table I.

TABLE I AROUND HERE

Following the procedure outlined above one may select a reference point in coordinate space and proceed straightforwardly to the computation of the clusters defining the cluster expansion. Instead of this, the PES expansion is defined in terms of $M = 10$ reference points and the weight in Eq. (42) takes the form

$$w(\mathbf{q}) = \frac{1}{M} \sum_{l=1}^{M} \delta(\mathbf{q} - \mathbf{a}_l). \tag{50}$$

The reference points $\mathbf{a}_l$ are located on or very close to stationary points in the lowest energy regions of the PES. After Eq. (50) the PES expansion is given by

$$\tilde{V}_{tot}(\mathbf{Q}) = \frac{1}{M} \sum_{l=1}^{M} \tilde{V}_l(\mathbf{Q}). \tag{51}$$

The $\tilde{V}_l(\mathbf{Q})$ terms are given by Eqs. (46) and (47). The specific form of $\tilde{V}_l(\mathbf{Q})$ that has been used here is given by

$$\tilde{V}_l(\mathbf{Q}) = V_l^{(0)} + \sum_{i=1}^{5} V_{l,i}^{(1)}(Q_i) + \sum_{i=1}^{4} \sum_{j=i+1}^{5} V_{l,ij}^{(2)}(Q_i, Q_j) + V_{l,z23}^{(3)}(z, Q_2, Q_3), \tag{52}$$

where the modes $Q_1 \cdots Q_5$ have been defined above. The $V_l^{(0)}$ term is the energy at the reference geometry l. The $V_{l,i}^{(1)}$ terms are the intra-group potentials obtained by keeping the coordinates in other groups at the reference geometry l, while the $V_{l,ij}^{(2)}$ terms account for the group-group correlations. The potential with up to second-order terms gives already a very reasonable description of the system. The $V_{l,z23}^{(3)}$ term accounts for three-mode correlations between the displacement of the central proton, the distance between both water molecules and the angular wagging and rocking motions. Note that the primitive grids in each coordinate are the same irrespective of the reference point used to expand the potential. This

means that the average, Eq. (51), can be carried out before the dynamical calculations by summing over all the generated grids of the same coordinates for each reference geometry, involving no extra cost for the dynamics. The justification for the multi-reference approach lies on the nature of $H_5O_2^+$. The protonated water-dimer is a very floppy system featuring several equivalent minima and large amplitude motions that traverse low potential energy barriers. Thus, the amount of configurational space available to the system at low vibrational energies is already large and then it is not well covered by a single reference point. The property that, for a single reference point, the PES expansion is exact at the reference point and hypersurfaces involving the displacement of up to h_m modes is lost after averaging over several reference geometries. However, the overall mean error is reduced by the averaging.

The use of several reference points has a further implication which is related to the symmetry properties of the system Hamiltonian. In the case of $H_5O_2^+$ a possible single reference geometry to define the PES expansion would be one of the eight equivalent absolute minima which belong to the $\mathcal{C}_2$ point groups. This choice, however, breaks the total symmetry of the Hamiltonian. We have seen that cut-HDMR is exact at the reference point and all hypersurfaces in which up to h_m modes have been displaced from the reference point, where h_m is the expansion order in terms of CC. The description of the rest of $\mathcal{C}_2$ points when one is used as a reference is thus not equivalent and the whole symmetry is broken. A possible solution would be to use as reference one of the two equivalent $\mathcal{D}_{2d}$ stationary points, which lie around 300 cm^{-1} above the absolute $\mathcal{C}_2$ minima. They correspond to $\alpha = 90$ or 270 degrees, respectively. Using only one of the $\mathcal{D}_{2d}$ points as reference results in a similar breakage of the total symmetry of the Hamiltonian. The same happens again if one of the two equivalent $\mathcal{D}_{2h}$ ($\alpha = 0$ or 180 deg.) stationary points is used, which are even higher in energy. One should note that this is a highly symmetrical, multiminima system in which several permutations of identical particles are possible through crossing of low energy conformational barriers. The vibrational levels of $H_5O_2^+$ can be labeled according to the permutation-inversion symmetry group $\mathcal{G}_{16}$ [39, 40], which contains the $\mathcal{D}_{2d}$ point group as a subgroup, but additionally allows to permute the H-atoms of either of the two monomers. The two $\mathcal{D}_{2d}$ and eight equivalent $\mathcal{C}_2$ geometries which are used as reference points are depicted in Fig. 4. The difference between the structures at the left and right columns is a 180 degrees rotation of α, or equivalently the permutation of the two hydrogens of one of the water moieties. The way out of the symmetry breakage problem is to use all the structures depicted in Fig. 4 as reference

points of the cluster expansion. The final potential is given then, as discussed above, by the average with respect to all the reference points. By using this set of reference points the symmetry of the original PES is maintained. Indeed, it will be maintained as long as, for an arbitrary selected reference geometry, all the symmetry equivalent points generated by the permutations-inversions of the $\mathcal{G}_{16}$ group are also considered as reference points.

FIGURE 4 AROUND HERE

IV. RESULTS AND DISCUSSION

A. Quantum Dynamical Calculations

The kinetic energy and potential energy operators already discussed are used to compute the zero point energy (ZPE) of the system and the corresponding ground-state vibrational-wavefunction. The algorithm that implements the computation of eigenvalues and eigenfunctions of the system Hamiltonian within the MCTDH program is called *improved relaxation* and is described elsewhere [41]. This algorithm is essentially a multiconfiguration self-consistent field approach that takes advantage of the MCTDH machinery. All the reported simulations were performed with the Heidelberg MCTDH package of programs [42].

The comparison between the largest, converged MCTDH calculation and other reported results on the same PES is given in Table II. As a reference we take the given diffusion Monte Carlo (DMC) result [12] which has an associated statistical uncertainty of 5 cm^{-1}. A simple normal-modes analysis (NMA) with normal modes constructed from the Hessian matrix taken at the $\mathcal{C}_2$ minimum yields a ZPE of 12 635 cm^{-1}, *only* 242 cm^{-1} larger than the DMC result. We believe that this surprisingly good result arises from fortuitous error cancellation. As will be discussed below, 3 out of the 15 internal degrees of freedom (γ_a, γ_b and α) are not described by a single-well in the lowest energy region of the potential, while the proton-transfer motion (z) features a nearly quartic potential which is strongly coupled to the water-water stretching (R). The most comprehensive calculations on the vibrational ground state based on a wavefunction approach to date are those of Bowman and collaborators [12] using the Multimode program [18]. The vibrational configuration interaction (VCI) results, both using the single reference (SR) and reaction path (RP) variants are found in Table II. These calculations use a normal-mode based Hamiltonian. They incorporate correlation

between the different degrees of freedom due to the cluster expansion of the potential [18] and the use of a CI wavefunction. The best reported VCI result for the ZPE lies still 104 cm^{-1} above the DMC value. It is worth to mention that before switching to a Hamiltonian based on polyspherical coordinates we tried a Hamiltonian expressed in rectilinear-coordinates and obtained results similar to those of Bowman and collaborators.

TABLE II AROUND HERE

The MCTDH converged result for the ZPE is given in Table II. The obtained value for the ZPE is 12 376.3 cm^{-1}, 16.7 cm^{-1} below the DMC value. Table III contains ZPE values obtained using an increasing number of configurations. According to these results the MCTDH reported values are assumed to be fully converged with respect to the number of configurations. The deviation from the DMC result must be attributed to the cluster expansion of the potential, Eqs. (51,52).

TABLE III AROUND HERE

We give here some technical details regarding the largest MCTDH calculation with 10 500 000 configurations, which is probably one of the largest MCTDH calculations performed to date in terms of required computational resources. The calculation was made using the recent parallel version of the MCTDH code which is still under development in our group. The calculation was run on a 8-processor, shared-memory machine with Intel Itanium2 processors, and used a total amount of 13.5 Gb of main memory. 4 Gb were devoted to storage of the Krylov vectors and Krylov times Hamiltonian vectors of the Davidson diagonalization procedure. The rest was needed for the representation of the Hamiltonian and the mean fields, the vector of coefficients, SPFs and work arrays. Each step of the wavefunction relaxation lasted around 13.5 hours of wall-clock time, and consisted of the aforementioned Davidson diagonalization of the system Hamiltonian in the current basis of SPFs followed by a 2 fs imaginary-time propagation of the SPFs. The whole procedure was iterated until self-consistency of the expansion coefficients and SPFs was reached.

In contrast, the smallest calculation reported in Table III, which used 172 800 configurations, consumed a total amount of memory of around 263 Mb. Each diagonalization of the system Hamiltonian plus imaginary time propagation of the SPFs lasted 10 minutes of wall clock time using two processors in parallel on the same Intel Itanium2 cluster. The

comparison of the two aforementioned simulations illustrates one of the major strengths of MCTDH, namely, the usage of variationally optimal coefficients and orbitals leads to an early convergence with respect to the size of the multiconfigurational expansion. Relatively good results (only 7.4 cm^{-1} energy difference between the largest and smallest calculation) are already obtained using very moderate computational resources.

B. Properties of the ground state of the system

The probability density of the ground state wavefunction with respect to some selected coordinates and integration over the remaining coordinates is given in Fig. 5. Fig. 5a shows the density along the proton-transfer coordinate z. The probability density is non negligible in a range spanning about 1 bohr. Fig. 5b depicts the density along the α internal rotation coordinate. Along this coordinate the system interconverts between two equivalent regions of configurational space. The barrier corresponds to planar configurations of the whole system and is about 300 cm^{-1} high depending on the configuration of the rest of coordinates. The system can interconvert between both halves even when in the ground vibrational state. The dotted curve in Fig. 5b depicts the density at a 10 times enlarged scale and clearly shows a non vanishing density for $\alpha = 0, \pi$. The splitting state arising from the barrier along α has also been computed and the splitting energy has been found to be 1 cm^{-1}. The small asymmetry observed in the density in Fig. 5b has been analyzed. It arises from the fact that the position of the proton is defined relative to one of the two water monomers, monomer A, in order to have 15 internal coordinates (see Eq. (10) and related text). Consequently, a change in α rotates the central proton so that its relative position to monomer A remains unaltered. In contrast, in order for the relative position of the central proton and monomer B to remain unaltered during a change in α, coordinates x and y must change accordingly. We emphasize that the kinetic operator is still exact and not affected by this. However, α, x and y coordinates are defined on non-matching grids. The total symmetry between monomers A and B with respect to the central proton is conserved in the case of a continuous configurational space instead of a discretized one. Thus, symmetry is slightly broken due to discretization of the configurational space. Energetically, the effect of this symmetry breakage must be well below 1 cm^{-1} which is the splitting caused by the barrier along α, since a larger perturbation would localize the density on one side of the

barrier breaking the double well feature. A perfect symmetry after discretization of the coordinates would probably be obtained if one switches to cylindrical coordinates (z, ρ, ϕ) for the proton and uses identical grids for the angles α and ϕ.

Fig. 5c shows the probability density along the wagging coordinates. It consists of four equivalent maxima, each of them centered at around ± 30 degrees from the planar water configuration, so that both water molecules are in pyramidal configuration. The probability density corresponding to one of the two water molecules in a planar configuration is however quite large and indicates a high probability of exchange between equivalent configurations of the system in which the water molecules switch between pyramidal geometries. Each of these four density maxima corresponds roughly to one of the $\mathcal{C}_2$ equivalent minima on the PES. A total of 8 equivalent $\mathcal{C}_2$ minima are present since the barrier along coordinate α divides the configurational space in two equivalent halves. When both monomers are in planar configuration the system interconverts between both $\mathcal{D}_{2d}$ and $\mathcal{D}_{2h}$ configurations by rotation along α.

FIGURE 5 AROUND HERE

Only after the introduction of a Hamiltonian based on polyspherical coordinates a satisfactory description the $H_5O_2^+$ cation was possible. The use of polyspherical coordinates allows for the characterization of the system in terms of well defined stretching, bending, rocking, wagging and internal rotation motions, each of which corresponds to *a single* coordinate. This fact keeps the correlation between coordinates in the PES relatively small, and the relation between different coordinates can be usually understood in simple physical terms. The representation of the WF given in these coordinates converges then more quickly than a WF constructed from rectilinear coordinates and can be more compact. The price to pay, however, is a much more complicated expression for the kinetic energy operator.

C. Quality of the PES expansion

In order to illustrate the convergence of the mode-combination based cluster-expansion PES introduced in Section III C the expectation values of the different terms of the potential are calculated for the ground vibrational state. These values are given in cm^{-1} in Table IV. The sum of the first order $\langle \Psi_0 | V^{(1)}(Q_i) | \Psi_0 \rangle$ terms is close to 6800 cm^{-1}, half the ZPE,

indicating that they carry the major weight in the description of the PES. The second order clusters introduce the missing correlation between modes. They have expectation values one order of magnitude smaller than the first order terms with one exception, the matrix element arising from the $V^{(2)}(Q_1, Q_2)$ potential. This can be easily understood by noting that modes Q_1 and Q_2 contain coordinates z and R, respectively. These two coordinates are strongly correlated and indeed they would be good candidates to be put in the same mode in an alternative mode-combination scheme. The only third order term that was introduced presents a rather marginal contribution to the potential energy of the system. These values prove that the PES representation used is of a good quality and rather well converged with respect to the reference PES, at least for the energy domain of interest. The square root of the expectation value of the potential squared is depicted in the third column. It is a measure of the dispersion around the expectation value and should also ideally vanish. The values indicate that the PES representation is good, albeit not yet fully converged. Some more terms of higher than second order may be added in the future as computational resources allow for it.

TABLE IV AROUND HERE

To finish the discussion it is worth mentioning that we have recently started to test a new mode-combination. It is based on 6 modes instead of 5. The definition of the modes in terms of the coordinates is as follows: $\tilde{Q}_1 = [z, R]$, $\tilde{Q}_2 = [x, y, \alpha]$, $\tilde{Q}_3 = [\gamma_A, \gamma_B]$, $\tilde{Q}_4 = [u_{\beta_A}, u_{\beta_B}]$, $\tilde{Q}_5 = [R_{1A}, R_{2A}, u_{\theta_{1A}}]$ and $\tilde{Q}_6 = [R_{1B}, R_{2B}, u_{\theta_{1B}}]$. At the beginning we started with 5 modes in order to keep the number of configurations as small as possible. This has the drawback that one of the combined modes, $Q_1 = [z, \alpha, x, y]$ is very large, thus its SPFs are harder to propagate. However, in the reported calculations we use the parallel version of the MCTDH code, and the parts which can be parallelized most efficiently are those involved with the vector of coefficients. Thus, a 6-modes scheme seems to be more efficient when the parallel code is used. In the 6-modes scheme we include all the first, second and some selected third order clusters. The obtained values of the ZPE are still preliminary but located in the region of -10 cm^{-1} with respect to DMC, in good accordance to the results of the 5-mode scheme. Such results indicate indeed that the reported simulations are robust with respect to the mode-combination scheme.

V. SUMMARY AND CONCLUSION

The protonated water-dimer ($H_5O_2^+$) is studied in its full dimensionality (15D) by quantum-dynamical wavefunction-methods, using the MCTDH approach. A set of curvilinear coordinates is used which accounts for the fluxional, multi-minima nature of the cation. An exact expression for the kinetic energy operator of the system is derived using the polyspherical method. A discussion of the different steps involved in the derivation is given. The set of polyspherical coordinates introduced allows the description of the different motions of the system, namely proton transfer, water-water stretching, OH stretchings, bendings and internal rotation by a single coordinate each which also have clear geometrical meanings in terms of angles or distances. The PES used in the calculations is that of Huang et al., the most accurate PES available for this system to date. The PES must be represented in a numerically and computationally adequate way for the quantum-dynamical simulations on a discrete multidimensional grid to be feasible. To this end, a variation of the hierarchical cut-HDMR method is presented which takes advantage of the mode-combination strategy used to represent the wavefunction. Combined modes, instead of the coordinates, are used to define the hierarchical expansion. The expansion of the PES is seen to converge quickly with the number of clusters in the expansion, which can be attributed to two factors:

1. A large amount of the correlation is already captured within the modes, which leads to quick convergence of the PES with respect to the number of clusters in the expansion.

2. The set of polyspherical coordinates used allows for the definition of physically meaningful modes avoiding at the same time artificial correlations (which are due to inadequate coordinates) to appear both in the potential energy and wave function.

The ZPE of the system is calculated and the results obtained show an excellent agreement with previous DMC calculations on the same PES. The reported ZPE with MCTDH lies only 16.7 cm^{-1} below the reported DMC result. This deviation from the "exact" DMC result (statistical error 5 cm^{-1}) must be due to the potential representation, as the KEO is exact and as it is shown, the reported ZPE is converged with respect to the number of configurations in the MCTDH expansion. A fully converged MCTDH calculation needs a rather large amount of computational resources, however, it is shown that reasonably good results are obtained with a much smaller configurational space due to the optimality of

both the coefficients and the SPFs in the MCTDH expansion. The properties of the ground vibrational state are analyzed. The central proton delocalizes on a range of about 1 bohr along the water-water axis. The fluxional nature of the system is exemplified in the probability density along the wagging γ_A and γ_B coordinates. The 2D space spanned by these coordinates presents four density maxima which roughly correspond to the $\mathcal{C}_2$ minima of the system. In going between different higher density regions the system switches between pyramidal conformations of the water molecules. These conformational changes take place along low potential-energy barriers. The system is completely delocalized over these low barriers leading to a highly symmetric ground-state wave function. The internal rotation coordinate α is seen to divide the configurational space in two equivalent halves. The probability density for $\alpha = 0$ and $\alpha = \pi$ (planar $\mathcal{D}_{2h}$) is non-negligible for the ground vibrational state. The tunneling splitting arising from the barrier along α is computed to be 1 cm^{-1}. The convergence of the PES expansion is monitored with respect to the expectation values of the potential-energy terms which define it, i.e. by inspecting $\langle\Psi_0|V_{ij\ldots}|\Psi_0\rangle$ and $\langle\Psi_0|V^2_{ij\ldots}|\Psi_0\rangle^{1/2}$. A good convergence is observed at second order with respect to the combined modes. The only third order term present has a rather marginal contribution to the energy with respect to $|\Psi_0\rangle$. Only after switching to curvilinear coordinates the fluxional motion of the highly symmetrical $H_5O_2^+$ cation was correctly accounted for.

The present paper has focused on the definition of an adequate set of coordinates and the derivation of the expression of the kinetic energy using the polyspherical method. A convenient way to represent the PES for high-dimensional quantum-dynamical simulation has been also discussed. The validity of the Hamiltonian setup has been established by comparison to available DMC results in the literature. Moreover, the properties of the ground vibrational state have been investigated. Our study provides a picture of the $H_5O_2^+$ system, in which the cluster has to be viewed as highly anharmonic, flexible, multi-minima, coupled system. We show that a converged quantum-dynamical description of such a complex molecular system can still be achieved. The companion paper following this one focuses on the infrared spectroscopy and dynamics of $H_5O_2^+$.

VI. ACKNOWLEDGMENTS

The authors thank Prof. J. Bowman for providing the potential-energy routine, M. Brill for the help with the parallelized code, and the Scientific Supercomputing Center Karlsruhe for generously providing computer time. O. V. is grateful to the Alexander von Humboldt Foundation for financial support. Travel support by the Deutsche Forschungsgemeinschaft (DFG) is also gratefully acknowledged.

---

[1] K. R. Asmis, N. L. Pivonka, G. Santambrogio, M. Brummer, C. Kaposta, D. M. Neumark, and L. Woste, Science **299**, 1375 (2003).

[2] T. D. Fridgen, T. B. McMahon, L. MacAleese, J. Lemaire, and P. Maitre, J. Phys. Chem. A **108**, 9008 (2004).

[3] J. M. Headrick, J. C. Bopp, and M. A. Johnson, J. Chem. Phys. **121**, 11523 (2004).

[4] N. I. Hammer, E. G. Diken, J. R. Roscioli, M. A. Johnson, E. M. Myshakin, K. D. Jordan, A. B. McCoy, J. M. Bowman, and S. Carter, J. Chem. Phys. **122**, 244301 (2005).

[5] J. M. Headrick, E. G. Diken, R. S. Walters, N. I. Hammer, R. A. Christie, J. Cui, E. M. Myshakin, M. A. Duncan, M. A. Johnson, and K. D. Jordan, Science **308**, 1765 (2005).

[6] J. R. Roscioli, L. R. McCunn, and M. A. Johnson, Science **316**, 249 (2007).

[7] X. Huang, B. J. Braams, and J. M. Bowman, J. Chem. Phys. **122**, 044308 (2005).

[8] M. V. Vener, O. Kühn, and J. Sauer, J. Chem. Phys. **114**, 240 (2001).

[9] J. Dai, Z. Bacic, X. C. Huang, S. Carter, and J. M. Bowman, J. Chem. Phys. **119**, 6571 (2003).

[10] J. Sauer and J. Dobler, Chem. Phys. Chem. **6**, 1706 (2005).

[11] M. Kaledin, A. L. Kaledin, and J. M. Bowman, J. Phys. Chem. A **110**, 2933 (2006).

[12] A. B. McCoy, X. Huang, S. Carter, M. Y. Landeweer, and J. M. Bowman, J. Chem. Phys. **122**, 061101 (2005).

[13] B. Podolsky, Phys. Rev. **32**, 812 (1928).

[14] F. Gatti, C. Iung, M. Menou, Y. Justum, A. Nauts, and X. Chapuisat, J. Chem. Phys. **108**, 8804 (1998).

[15] F. Gatti, J. Chem. Phys. **111**, 7225 (1999).

[16] F. Gatti, C. Munoz, and C. Iung, J. Chem. Phys. **114**, 8275 (2001).

[17] F. Gatti and C. Iung, J. Theor. Comp. Chem. **2**, 507 (2003).

[18] J. M. Bowman, S. Carter, and X. Huang, Int. Rev. Phys. Chem. **22**, 533 (2003).

[19] H. Rabitz and O. F. Alis, J. Math. Chem. **25**, 197 (1999).

[20] G. Li, S. Wang, C. Rosenthal, and H. Rabitz, J. Math. Chem. **30**, 1 (2001).

[21] O. Vendrell, F. Gatti, and H.-D. Meyer, J. Chem. Phys. (2007).

[22] H.-D. Meyer, U. Manthe, and L. S. Cederbaum, Chem. Phys. Lett. **165**, 73 (1990).

[23] U. Manthe, H.-D. Meyer, and L. S. Cederbaum, J. Chem. Phys. **97**, 3199 (1992).

[24] M. H. Beck, A. Jäckle, G. A. Worth, and H.-D. Meyer, Phys. Rep. **324**, 1 (2000).

[25] H.-D. Meyer and G. A. Worth, Theor. Chem. Acc. **109**, 251 (2003).

[26] F. Gatti, C. Iung, M. Menou, and X. Chapuisat, J. Chem. Phys. **108**, 8821 (1998).

[27] C. Iung, F. Gatti, A. Viel, and X. Chapuisat, PCCP **1**, 3377 (1999).

[28] C. Leforestier, F. Gatti, R. S. Fellers, and R. J. Saykally, J. Chem. Phys. **117**, 8710 (2002).

[29] F. Gatti and A. Nauts, Chem. Phys. **295**, 167 (2003).

[30] D. Lauvergnat and A. Nauts, J. Chem. Phys. **116**, 8560 (2002).

[31] A. Jäckle and H.-D. Meyer, J. Chem. Phys. **104**, 7974 (1996).

[32] A. Jäckle and H.-D. Meyer, J. Chem. Phys. **109**, 3772 (1998).

[33] O. F. Alis and H. Rabitz, J. Math. Chem. **29**, 127 (2001).

[34] G. Y. Li, J. S. Hu, S. W. Wang, P. G. Georgopoulos, J. Schoendorf, and H. Rabitz, J. Phys. Chem. A **110**, 2474 (2006).

[35] S. Manzhos and T. Carrington, J. Chem. Phys. **125**, 084109 (2006).

[36] S. W. Wang, P. G. Georgopoulos, G. Y. Li, and H. Rabitz, J. Phys. Chem. A **107**, 4707 (2003).

[37] A. Chakraborty, D. G. Truhlar, J. M. Bowman, and S. Carter, J. Chem. Phys. **121**, 2071 (2004).

[38] G. J. Kroes and H.-D. Meyer, Chem. Phys. Lett. **440**, 334 (2007).

[39] D. J. Wales, J. Chem. Phys. **110**, 10403 (1999).

[40] P. R. Bunker and P. Jensen, *Molecular Symmetry and Spectroscopy* (NRC Research Press, 1998), 2nd ed.

[41] H.-D. Meyer, F. Le Quéré, C. Léonard, and F. Gatti, Chem. Phys. **329**, 179 (2006).

[42] G. A. Worth, M. H. Beck, A. Jäckle, and H.-D. Meyer, The MCTDH Pack-

age, Version 8.2, (2000). H.-D. Meyer, Version 8.3 (2002), Version 8.4 (2007). See http://www.pci.uni-heidelberg.de/tc/usr/mctdh/.

TABLE I: Definition of the one-dimensional grids. N denotes the number of grid points and x_i, x_f the location of first and last point. The DVRs are defined in Appendix B of Ref. [24].

Coord.	N	x_i	x_f	DVR
z	27	-1.8	1.8	HO
α	21	0	2π	exp
x	5	-0.9	0.9	HO
y	5	-0.9	0.9	HO
R	16	4.2	6.5	HO
u_{β_A}	7	-0.5	0.5	sin
u_{β_B}	7	-0.5	0.5	sin
γ_A	19	π-1.8	π+1.8	sin
γ_B	19	-1.8	1.8	sin
R_{1A}	9	0.5	1.8	HO
R_{2A}	9	2.2	3.8	HO
$u_{\theta_{1A}}$	7	-0.5	0.5	sin
R_{1B}	9	0.5	1.8	HO
R_{2B}	9	2.2	3.8	HO
$u_{\theta_{1B}}$	7	-0.5	0.5	sin

TABLE II: Comparison of the zero point energy (ZPE) of the $H_5O_2^+$ cation calculated by various approaches on the PES by Huang et. al.[7]: diffusion Monte-Carlo (DMC), normal mode analysis (harmonic), vibrational CI single reference (VCI-SR) and reaction path (VCI-RP) as published in [12] and MCTDH results. Δ denotes the difference to the DMC result. The converged MCTDH result is obtained with 10 500 000 configurations. Compare with Table III.

Method	ZPE(cm^{-1})	Δ(cm^{-1})
DMC	12 393	0
harmonic	12 635	242
VCI-SR	12 590	197
VCI-RP	12 497	104
MCTDH	12 376.3	−16.7

TABLE III: Comparison of the zero point energy (ZPE) of the $H_5O_2^+$ cation between different MCTDH calculations with ascending number of configurations. The Δ values are given with respect to the diffusion Monte Carlo result, 12 393 cm^{-1} [12].

SPFs per Mode	N configs.	ZPE(cm^{-1})	Δ(cm^{-1})
$(20, 20, 12, 6, 6)$	172 800	12 383.7	-9.3
$(35, 25, 15, 8, 8)$	840 000	12 378.5	-14.5
$(40, 40, 20, 8, 8)$	2 048 000	12 377.8	-15.2
$(60, 40, 20, 8, 8)$	3 072 000	12 376.7	-16.3
$(70, 50, 30, 10, 10)$	10 500 000	12 376.3	-16.7

TABLE IV: Expectation value of the different terms of the potential expansion (central column) and square root of the expectation value of the potential squared (right column). All energies in cm^{-1}. The combined modes read: $Q_1 = [z, \alpha, x, y]$, $Q_2 = [\gamma_A, \gamma_B]$, $Q_3 = [R, u_{\beta_A}, u_{\beta_B}]$, $Q_4 = [R_{1A}, R_{2A}, u_{\theta_{1A}}]$ and $Q_5 = [R_{1B}, R_{2B}, u_{\theta_{1B}}]$.

	$\langle\Psi_0\|V\|\Psi_0\rangle$	$\langle\Psi_0\|V^2\|\Psi_0\rangle^{1/2}$
$V^{(1)}(Q_1)$	1293.6	1807.7
$V^{(1)}(Q_2)$	750.6	966.9
$V^{(1)}(Q_3)$	171.5	266.9
$V^{(1)}(Q_4)$	2293.2	3062.8
$V^{(1)}(Q_5)$	2293.1	3062.8
$V^{(2)}(Q_1, Q_2)$	-526.9	1037.2
$V^{(2)}(Q_1, Q_3)$	-78.8	290.2
$V^{(2)}(Q_1, Q_4)$	-27.5	231.8
$V^{(2)}(Q_1, Q_4)$	-27.4	231.7
$V^{(2)}(Q_2, Q_3)$	-10.5	37.6
$V^{(2)}(Q_2, Q_4)$	-24.7	117.5
$V^{(2)}(Q_2, Q_5)$	-24.7	117.9
$V^{(2)}(Q_3, Q_4)$	-18.8	180.9
$V^{(2)}(Q_3, Q_5)$	-18.8	180.9
$V^{(2)}(Q_4, Q_5)$	1.2	9.9
$V^{(3)}(z, Q_2, Q_3)$	1.0	50.4

Figure Captions

Figure 1: Jacobi description of the $H_5O_2^+$ system. The vector $\vec{R}$ connects the two centers of mass of the water monomers. The vector $\vec{r}$ connects the center of mass of the water dimer with the central proton.

Figure 2: Definition of the angles for the $H_5O_2^+$ system. The angles α_A and α_B describe the rotation of the water monomers around the vector $\vec{R}$, or equivalently around the z-axis of the E2- or BF-frame.

Figure 3: Number of grid points needed for the representation of the clusters of the PES expansion. m is the number of coordinates making a mode. 10 grid points per coordinates and 15 coordinates are assumed. A horizontal line is drawn at 10^8, which tentatively signals the maximum practical number of points both regarding their calculation and the use of the grids in the dynamical calculations.

Figure 4: Geometries of the 10 reference points used in the PES expansion. The view is along the O-H-O axis. Hence only the closest of the two oxygen and the four hydrogens can be seen. The difference between the geometries in the left column and each geometry at the right column is a rotation of π along α. Equivalently, the pairs of structures (a,b), (c,j), (e,h), (g,f), (i,d) are related by a permutation of hydrogen atoms of one of the monomers. The following coordinates are identical for all reference points: $R = 4.70$ au, $x, y, z = 0$, $R_{1(A,B)} = 1.07$ au, $R_{2(A,B)} = 2.98$ au, $\theta_{1A(1B)} = 0$, $u_{\beta_{A(B)}} = 0$. Only coordinates α, γ_A and γ_B differ at the 10 reference points.

Figure 5: For the ground vibrational state probability density along selected coordinates and integration over the rest: probability density along the z proton-transfer coordinate (a), along the α internal rotation coordinate (b) and on the 2D space spanned by the wagging γ_A and γ_B coordinates (c). The dotted line in (b) corresponds to a 10 times enlarged scale. It indicates that the probability density at $\alpha = \pi$ is not vanishing.

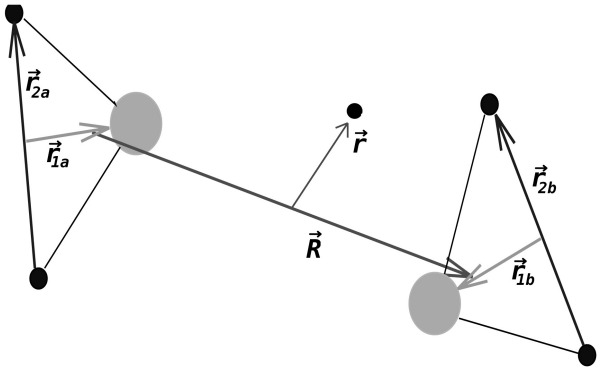

FIG. 1: Vendrell et. al., Journal of Chemical Physics

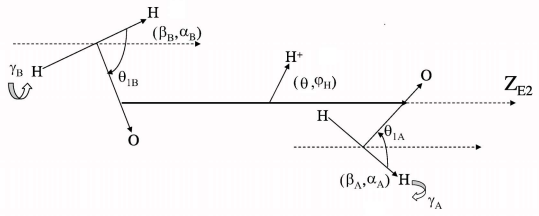

FIG. 2: Vendrell et. al., Journal of Chemical Physics

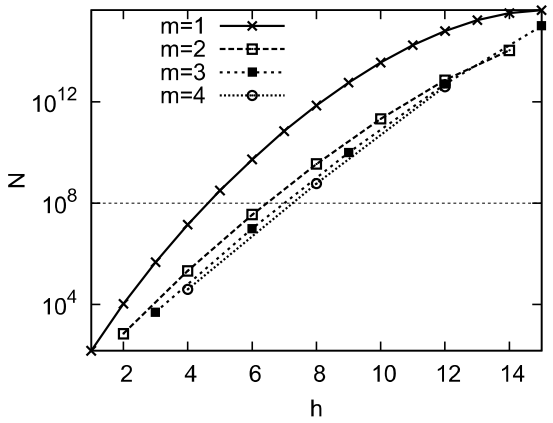

FIG. 3: Vendrell et. al., Journal of Chemical Physics

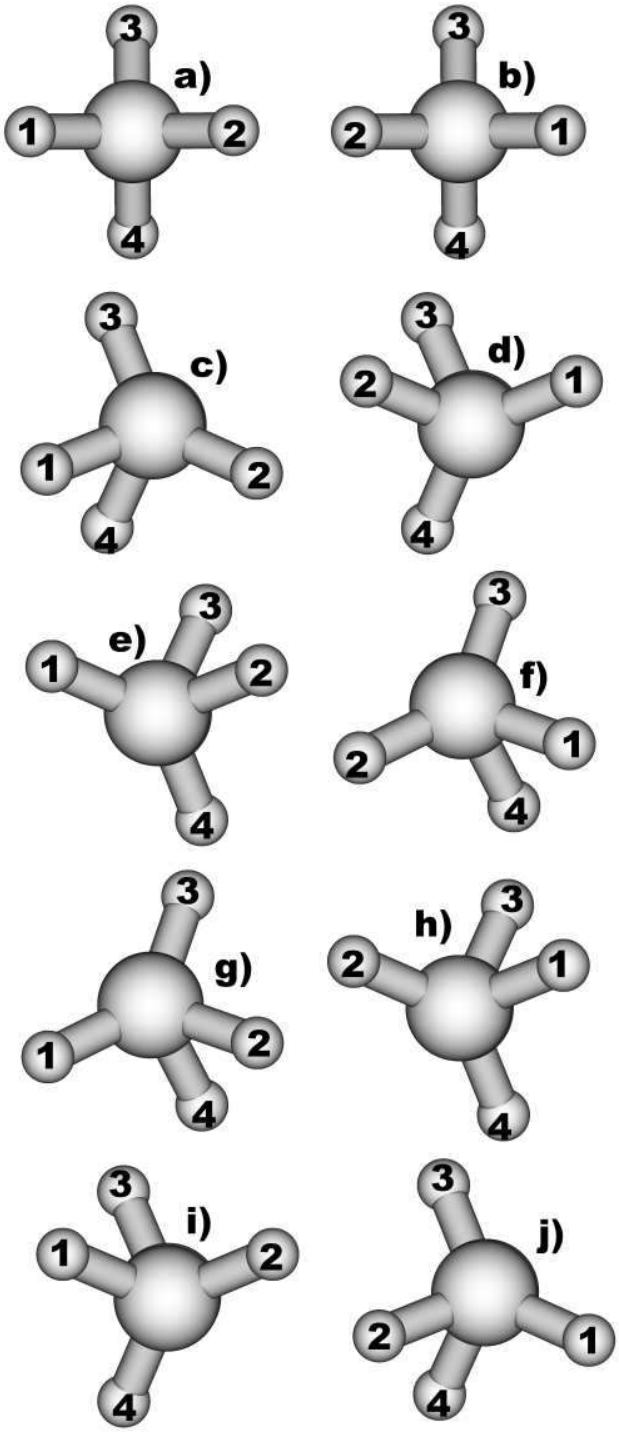

FIG. 4: Vendrell et. al., Journal of Chemical Physics

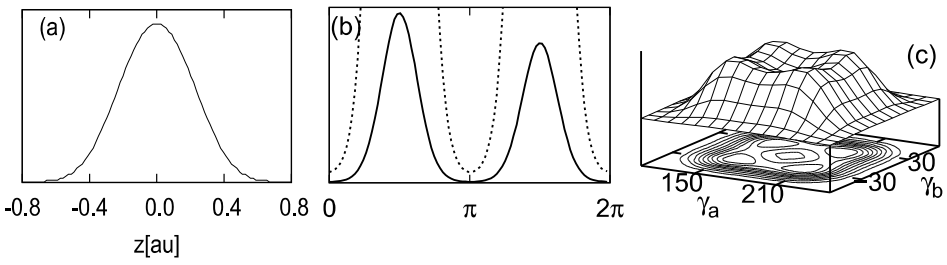

FIG. 5: Vendrell et. al., Journal of Chemical Physics